Published in final edited form as:

ACS Nano. 2016 May 24; 10(5): 5070–5085. doi:10.1021/acsnano.5b08218.

Translocation of Functionalized Multi-Walled Carbon Nanotubes across Human Pulmonary Alveolar Epithelium: Dominant Role of Epithelial Type 1 Cells

Pakatip Ruenraroengsak[1,2,*], **Shu Chen**[1], **Sheng Hu**[3], **Jodie Melbourne**[1], **Sinbad Sweeney**[2], **Andrew J. Thorley**[2], **Jeremy N. Skepper**[4], **Milo S. P. Shaffer**[3], **Teresa D. Tetley**[2,*], **Alexandra E. Porter**[1,*]

[1]Department of Materials and London Centre for Nanotechnology, Imperial College London, Exhibition Road, London, UK, SW7 2AZ.

[2]Lung Cell Biology, Airways Disease, National Heart and Lung Institute, Imperial College London, Dovehouse Street, London, UK, SW3 6LY.

[3]Department of Chemistry and London Centre for Nanotechnology, Imperial College London, Exhibition Road, London, UK.

[4]Cambridge Advanced Imaging Centre, Department of Physiology, Development and Neuroscience, University of Cambridge, UK, CB2 3DY.

[*]Correspondence should be addressed to: Dr Pakatip Ruenraroengsak, Department of Materials and London Centre for Nanotechnology, Imperial College London, London SW7 2AZ, UK, preunrar@ic.ac.uk; Prof. Teresa D. Tetley, Department of Lung Cell Biology, National Heart and Lung Institute, Guy Scadding Building, Dovehouse Street, London SW3 6LY, UK Phone: +44-207-5942984, t.tetley@imperial.ac.uk; Dr Alexandra E. Porter, Department of Materials and London Centre for Nanotechnology, Imperial College London, London SW7 2AZ, UK, Phone: +44-207-594691, a.porter@imperial.ac.uk.

Author Contributions

TDT, MSPS and AEP conceived and designed the project. PR designed and PR, SH, HC, JM, SS, AJT performed the experiments. The manuscript was written by PR and revised with TDT, MSPS and AEP, with contributions from all authors. All authors discussed the results and commented on the manuscript. All authors have given approval to the final version of the manuscript.

Notes

Work carried out to obtain the primary human alveolar epithelial type 2 cells was approved by the Royal Brompton and Harefield Ethical committee (Reference: 08/H0708/73). The authors declare no competing financial interest.

ASSOCIATED CONTENT

Supporting Information (SI)

Details of materials and methods (listed below), the results of electrical cell-substrate impedance sensing (ECIS system), and the results of Raman spectroscopy measurement are available free of charge *via* the Internet at http://pubs.acs.org.

Materials and methods of MWCNT synthesis, surface functionalization, characterization and endotoxin analysis. Methods of Raman spectroscopy and the evaluation TEER data using Electric Cell-substrate Impedance Sensing (ECIS system).

Figure S1. Model study, functionalization and shortening process of p(4VP)-MWCNTs

Figure S2. Effect of p(4VP)-MWCNTs on TT1 (n=3 experiments) and AT2 cell (n=6 subject samples) viability

Figure S3. Effects of p(4VP)-MWCNTs on inflammatory mediator release, IL-6 and IL-8, by TT1 and AT2 cells

Figure S4. Cell impedance and TEER profiles of TT1 cells exposed to p(4VP) for 24h Figure S5.

Degree of agglomeration or aggregation of 300nm and 700nm long, p(4VP)-MWCNTs

Figure S6. The p(4VP)-MWCNTs penetrated the lysosomal membrane of TT1 cells and Raman spectroscopy

SV1. Effect of p(4VP)-MWCNTs on tight junctions of TT1 cell monolayer

SV2. TT1 exposed to 300nm p(4VP)-MWCNTs for 24h were rinsing with PBS

SV3. TT1 exposed to 700nm p(4VP)-MWCNTs for 24h were rinsing with PBS

SV4. AT2 exposed to 300nm p(4VP)-MWCNTs for 24h were rinsing with PBS

SV5. AT2 exposed to 700nm p(4VP)-MWCNTs for 24h were rinsing with PBS

SV6. Localisation of 700nm p(4VP)-MWCNTs within lysosomal compartment within TT1 cells

SV7. Localisation of 700nm p(4VP)-MWCNTs within endosomal compartment within TT1 cells

SV8. Effect of p(4VP)-MWCNTs on tight junctions of AT2 cell monolayer

SV9. Localisation of 700nm p(4VP)-MWCNTs within endosomal compartment within AT2 cells

SV10. Localisation of 700nm p(4VP)-MWCNTs within lysosomal compartment within AT2 cells

Abstract

Uptake and translocation of short functionalised multi-walled carbon nanotubes (short-fMWCNTs) through the pulmonary respiratory epithelial barrier depend on physicochemical property and cell type. Two mono-culture models, immortalised human alveolar epithelial type 1 (TT1) cells and primary human alveolar epithelial type 2 cells (AT2), which constitute the alveolar epithelial barrier, were employed to investigate the uptake and transport of 300 and 700nm in length, poly(4-vinyl pyridine)-functionalized, multi-walled carbon nanotubes (p(4VP)-MWCNTs) using quantitative imaging and spectroscopy techniques. The p(4VP)-MWCNT exhibited no toxicity on TT1 and AT2 cells, but significantly decreased barrier integrity (*p<0.01). Uptake of p(4VP)-MWCNTs was observed in 70% of TT1 cells, correlating with compromised barrier integrity and basolateral p(4VP)-MWCNT translocation. There was a small but significantly greater uptake of 300nm p(4VP)-MWCNTs than 700nm p(4VP)-MWCNTs by TT1 cells. Up to 3% of both the 300 and 700nm p(4VP)-MWCNTs reach the basal chamber; this relatively low amount arose because the supporting transwell membrane minimized the amount of p(4VP)-MWCNT translocating to the basal chamber, seen trapped between the basolateral cell membrane and the membrane. Only 8% of AT2 cells internalised p(4VP)-MWCNT, accounting for 17% of applied p(4VP)-MWCNT), with transient effects on barrier function, which initially fell then returned to normal; there was no MWCNT basolateral translocation. The transport rate was MWCNT-length-modulated. The comparatively lower p(4VP)-MWCNT uptake by AT2 cells is proposed to reflect a primary barrier effect of type 2 cell secretions and the functional differences between the type 1 and type 2 alveolar epithelial cells.

Graphical Abstract

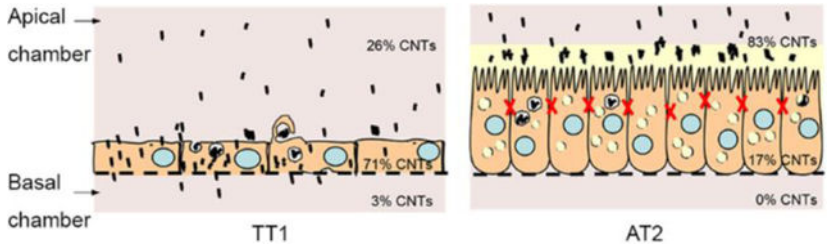

Keywords

Functionalized multi-walled carbon nanotubes; uptake; translocation; alveolar epithelial barrier; electron microscopy; quantitative imaging technique

Short, functionalized multi-walled carbon nanotubes (short-fMWCNTs) have attracted considerable industrial[1] and pharmaceutical[2,3] attention for a wide range of applications, including nanocomposite fillers[1] and drug delivery.[3] The increasing number of products containing MWCNTs may lead to environmental release and accidental exposure during manufacture, use or disposal of the products. Although inhalation of nanosized particles may have adverse effects,[4,5] relatively little is known about their chronic toxicity[6] or their ability to cross the gas-blood barrier to reach systemic sites, an important consideration in inhaled nanodrug delivery. The bioreactivity and toxicity of fMWCNTs is related to their physicochemical properties.[7] Functionalization reduces MWCNT toxicity and increases

their solubility enabling medical applications.[8] However, typical functionalization/dispersion processes cause damage or changes in the MWCNT dimensions that limit their performance. We have prepared highly consistent short-fMWCNTs[8] to investigate whether the 4-vinyl-pyridine-fMWCNTs (p(4VP)-MWCNTs) can cross the alveolar epithelial barrier, and if so, by which pathway(s) transport occurs. The grafting density of 4VP is very low but sufficient to alter zeta potential and water compatibility.[8] This treatment allows the production of stable aqueous dispersions of p(4VP)-MWCNTs, and hence the transport of individual MWCNTs can be studied. A systematic approach, using scanning electron microscopy (SEM) and high-resolution electron microscopy (HR-TEM), has been employed to investigate the nano-bio interface between the MWCNTs and the plasma membrane of the alveolar epithelial barrier. Importantly, this study is performed without using any labelling probes which could alter physicochemical properties and biological-interaction of MWCNTs.

The lung provides a large surface area for inhaled MWCNT deposition with extensive vascularization. In humans, inhaled nanoparticles with an aerodynamic diameter of <5μm are respirable, and it has been shown that individual, short-MWCNTs 10–165 nm in diameter (≤5 μm long), may reach the deep lung where alveolar macrophages will attempt to clear them.[9] However, very short MWCNTs may bypass the macrophages and interact directly with the alveolar epithelium, which consists of human alveolar epithelial type 1 (AT1), forming a thin layer (thickness of <250 nm), and cuboidal type 2 (AT2) cells,[10] both coated with lung lining fluid, a mixture of pulmonary surfactant and alveolar subphase fluid, 0.1–0.2 μm deep.[11] AT1 cells cover >95% of alveolar surface area, facilitating gas exchange and are susceptible to inhaled particles.[12] The AT2 cells are cuboidal secretory cells which release pulmonary surfactant (PS) to maintain the surface tension within the lung, as well as secreting surfactant-associated proteins and other molecules that assist in host defense. The differences between these two cell types in their tight junction formation, barrier integrity, permeability and bioreactivity will crucially influence the fate of inhaled CNTs and CNT-based drug design for pulmonary drug delivery and diagnostic use.

To date, there is no standard model of the human alveolar epithelium for characterizing the pharmacokinetics and toxicology of engineered nanomaterials *in vitro*; most previous studies have utilized cell lines and primary rodent lung cells.[13] In this study, *in vitro* mono-culture models (see methods) of two highly relevant cell types: a unique immortal human AT1 cell line (TT1,[12] derived from immortalised, primary human AT2 cells,[14] progenitors[15] of AT1 cells) and primary AT2 cells,[14] obtained from normal regions of human lung tissue, have been used to gain insight to events that would occur at the alveolar epithelial interface *in vivo*. Either TT1 or AT2 monolayers were grown on the apical side of transwell® membranes (polyester membrane (PE), pore diameter of 0.4μm; Supplementary Figure 1a (Figure S1a)). Monolayers were exposed to p(4VP)-MWCNTs or the graft polymer of poly-4-vinyl-pyridine, p(4VP), added to the apical chamber (Figure S1b), for 24h. Uptake and translocation of p(4VP)-MWCNTs into and through the cells were quantified *via* optical absorption of the apical and basal chamber fluids, cell lysates and statistical TEM analysis of the cell monolayers.

We have also explored the specific hypothesis that fundamental differences between TT1 and AT2 cells may alter the extent of p(4VP)-fMWCNT uptake and their subsequent transport across the alveolar barrier. In addition, although short-fMWCNTs ≤1μm are being investigated for multiple biomedical applications,[16,17] differences in bioreactivity, relating to length, are not yet clear. Chemical vapour deposition (CVD) grown, commercial MWCNTs were thermochemically grafted, to produce clean, fMWCNTs, with minimal framework damage.[18] As it is known that shorter/smaller particles are more likely to reach the lung epithelium, two different dispersed length fractions were prepared to determine any differential effects of length on cell behaviour. The 4VP functional group provides aqueous dispersion stability at very low levels of grafting, as well as being relevant to certain applications;[19] full details of synthesis and cellular toxicity have been reported previously,[8] as elaborated in supporting information (SI; Figure S1b–g). Following the addition of the individualised p(4VP)-MWCNTs to the apical chamber, their impact on cell bioreactivity was investigated by measuring cell viability, mitochondrial activity, cell membrane integrity (SI and Figure S2a–d) and inflammatory mediator release (SI and Figure S3); the impact on dynamic permeability was established by monitoring transepithelial electrical resistance (TEER), apical-basal dextran transport and tight junction integrity. The TEER measurement was further evaluated using an electric cell-substrate impedance sensing (ECIS) system and showed similar trends over a 24h exposure period (SI and Figure S4). The effect of p(4VP) was also investigated. The fate of individual and agglomerated p(4VP)-MWCNTs were systematically tracked by light microscopy (LM), transmission electron microscopy (TEM), HR-TEM, SEM and laser scanning confocal microscopy (CM) to capture dynamic events in live and fixed cells. The effects of length and surface chemistry of p(4VP)-MWCNTs on cell uptake were quantified for both TT1 and AT2 monolayers. An increase in TT1 cell uptake of the p(4VP)-fMWCNTs was also observed in comparison to the non-fMWCNTs (p-MWCNTs, Figure 6a). Since the non-fMWCNTs did not form a stable suspension in DCCM1 medium, it was not possible to analyse the transport. However, the viability (Figure S2) and TT1 cell uptake of the p-MWCNTs (Figure 6a) were analysed.

RESULTS

p(4VP)-MWCNTs Synthesis and Characterization

The pristine CVD-synthesized MWCNTs were functionalised with 4-vinyl pyridine (4VP) *via* an established thermochemical grafting method (SI; Figure S1a),[8] and well characterized as reported previously.[8] After the shortening process, the diameter of the p(4VP)-MWCNTs was 12.1±4nm (mean ± SD, Figure S1b–f). The mean length of the p(4VP)-MWCNTs decreased and the length distribution became narrow as sonication time increased. Supporting figure 1c (Figure S1c) shows the morphology of individualised MWCNTs before sonication with a length distribution of 0.66 ± 0.51 μm (Figure S1d–e). After 5 h sonication, the length of MWCNTs was significantly reduced (Figure S1e), and the final length distribution was 0.30 ± 0.18 μm (Figure S1f). The zeta potentials of the ~300 and ~700 nm p(4VP)-MWCNTs in water (pH7.0) were −6.25±1.4 and 1.12±0.3 mV (mean±SD), respectively, but changed in the cell culture medium (pH7.4) to −12.40±0.8 and −11.50±0.9 mV (mean±SD), respectively. An endotoxin test was performed on both the 300 and 700nm

p(4VP)-MWCNT samples and the endotoxin levels were found to be very low at 0.0940 ± 0.0047(SD) and 0.0281 ± 0.0056(SD) EU/ml, respectively.

Effects of p(4VP)-MWCNTs on Cell Viability and Inflammatory Mediator Release

The cytotoxicity of non-fMWCNT, 300 and 700nm long p(4VP)-MWCNTs was first evaluated using the water soluble tetrazolium derivative (WST) assay (cells; Figure S2a–b), and a lactate dehydrogenase (LDH) assay (conditioned medium; Figure S2b–c) for both TT1 and AT2 cells. All MWCNTs exhibited insignificant toxic effects ($p>0.05$) on TT1 and AT2 cells after 24 hours exposure to up to 30μg/ml. They also did not cause any significant ($p>0.001$) release of LDH by either cell type (Figure S2b–c), indicating that the non-fMWCNTs (p-MWCNTs) and p(4VP)-MWCNTs did not damage the cell membrane integrity. The effects of p(4VP)-MWCNTs on release of inflammatory mediators, IL-6 and IL-8, were also investigated (Figure S3); neither length of the MWCNTs caused significant ($p>0.001$, n=3(TT1) and n=6(AT2)) release of IL-6 and IL-8 from either TT1 or AT2 cells.

Effect of p(4VP)-MWCNTs on TEER, Dextran Permeability and Tight Junctions

TEER assesses the level of tight junction formation by measuring the Ohmic resistance of the cell barrier. Both cell types formed tight junctions (Figure 1a–d). The baseline TEER value trends measured from the TT1 and AT2 cells were consistent with previous studies[20,21] with TEER values for TT1 and AT2 of 56±3 (number of experiments, n=3) and 639±30 Ωcm^2 (number of subject samples and number of experiments, n=6) respectively (Figure 1a–b); the order of magnitude higher value for AT2 cells reflects the very deep, strong tight junctions developed by AT2 cells *in vitro*, approximately twice as deep TT1 cell tight junctions.[12,14] p(4VP) alone induced a sharp significant increase in TEER, $*p<0.01$, n=3(TT1) and n=6(AT2), following addition (at t=0.5–2h) and shortly returned to the base line (Figure 1c–d). p(4VP) also caused a significant increase in apical-basal-dextran transport at t=3h, $*p<0.01$, n=3 on the TT1 cells, but no significant change was observed on the AT 2 cells (Figure 1e–f). Exposure of both cell types, (Figure 1a–b), to 300nm and 700 nm p(4VP)-MWCNTs caused a significant reduction ($*p<0.01$, n=3), 10–21%, in TEER after 30 minutes for TT1 cells and 9–20% for AT2 cells. In comparison to the p(4VP) control at t=4–24h, the p(4VP)-MWCNT exhibited a significantly higher TEER reduction, on both cell types (Figure 1a–b). Interestingly, AT2 cells recovered their original TEER (Figure 1b) within 7h of exposure. In contrast, TT1 cell TEERs showed only a small recovery to a net 19% TEER reduction (t=24h) for 700nm p(4VP)-MWCNTs, while with 300nm p(4VP)-MWCNTs, TEER values continued drop (21–33%; Figure 1a–b).

The integrity of the monolayers was also probed using FITC-dextran 4000 (Sigma, UK), a marker of paracellular transport (Figure 1e–f). For short exposures (<4 h), the significant reduction ($**p<0.001$, n=3) of the TEER caused by the 300nm p(4VP)-MWCNT correlated with a significant ($**p<0.001$, n=3) increase in apical-basal dextran transport across the TT1 monolayer (Figure 1e). The tight junction protein, ZO-1, was observed by immuno fluorescent staining and imaging using CM. At 24h, exposure to p(4VP)-MWCNT (300 or 700 nm) reduced the intensity (Figure 2b, g) of the tight junctions within the TT1 monolayer, compared to control cells (Figure 2a). Although, the ZO-1 and p(4VP)-

MWCNTs did not co-localize (Supporting video 1; SV1), after 24h, the p(4VP)-MWCNTs disturbed tight junction formation between TT1 cells.

For AT2 cells, a slight but significant (*p<0.01) increase in apical-basal-dextran transport was observed between t=1.5–2h (Figure 1f) in cells exposed to 300nm p(4VP)-MWCNTs; although, both 300 and 700 nm p(4VP)-MWCNTs initially reduced the TEER (Figure 1d), the value completely recovered over time. This recovery may reflect the presence of a secreted surfactant layer, or, as mentioned earlier, strong tight junctions formed by AT2 cells (Figure 2j–k, o). The ZO-1 staining of tight junctions (Figure 2j–k, o) also shows no change in intensity or structure of AT2 cells exposed to p(4VP)-MWCNTs (24h). Pulmonary surfactant (PS) secreted by AT2 cells contains phospholipids (~80%), cholesterol (~10%) and surfactant proteins (SPs; ~10%).[11] SP-A and SP-D show similar roles to opsonins, promoting microbial clearance. Lipids and SPs have been reported to interact with or adsorb onto single and MWCNTs.[22,23] Dynamic translocation of cationic, neutral and anionic nanoparticles across the surfactant layer has been shown to be dependent on their hydrophobicity.[24] The p(4VP)-MWCNTs are relatively hydrophilic and should penetrate the surfactant quickly to reach the AT2 cells. However, following 30 min p(4VP)-MWCNTs exposure, the MWCNTs were observed to settle and adhere on top of the cell monolayer; degree of MWCNT agglomerates/aggregates was also observed (Figure S5 and SV 2–5) indicating that the p(4VP)-MWCNTs may interact with the lipids, or they adsorbed surfactant-associated proteins, notably SP-A and SP-D,[25] which are suggested to cause agglomeration of nanomaterials.[26,27] To determine the degree of MWCNT agglomerates/ aggregates we made the assumption that the majority of the extracellular agglomerated/ aggregated material would be loosely cell-associated, settled on the cell monolayer or within the apical secretions. We exposed the TT1 and AT2 cells to 300nm and 700nm p(4VP)-MWCNTs in length for 24h, and measured the concentrations of the MWCNTs remaining in suspension within the medium (removed at 24h, see details in methods) and that found within the subsequent rinsing solution (reflecting cell-associated or in secretions). The results are shown below, in Figure S5 and in a supporting video 2–5 and confirmed the results shown in the manuscript in Figure 6b, that approximately 77–80% of the MWCNTs applied to AT2 cells remained in the apical chamber and could be easily washed off (video 4–5); of this, 79% (300nm) and 94% (700nm) of MWCNTs observed were located in the rinsing solution, suggesting the presence of trapped MWCNTs and mostly agglomerates/ aggregates within the surfactant-rich washings. For TT1 cells, 22–25% of the exposed MWCNTs remained in the apical chamber; 7% (300nm) and 10% (700nm) of MWCNTs observed in apical chamber were in the rinsing solution (rich in agglomerates/aggregates as indicated in the video 2–3) and accounted for only 1.7% and 2.0% of the original 300nm and 700nm applied fMWCNTs.

Due to the percentage of MWCNT uptake, particularly by TT1, the degree of aggregation/ agglomeration was also investigated in a cell-free system using ‘conditioned media’ generated by pre-incubation the medium with TT1 or AT2 monocultures for 24h (see details in methods), to determine the degree of agglomeration/aggregation in the absence of cellular uptake. The degree of agglomeration/aggregation of the p(4VP)-MWCNTs in conditioned media was 22% and 31% (300nm and 700nm respectively) for TT1 conditioned medium (much the same as that for the non-conditioned culture medium, p>0.005, n=3) and 65% and

79% (300nm and 700nm respectively) for AT2 conditioned medium, suggesting that AT2 secretions significantly induce agglomeration/aggregation (***p<0.001, n=3, Figure S5e). Nevertheless, approximately 22% (300nm) and 31% (700nm) agglomeration/aggregation occurred in the TT1 conditioned medium, and 23% (300nm) and 32%(700nm) fMWCNT agglomerates/aggregates occurred in the non-conditioned medium, indicating that TT1 cell secretions have little influence on MWCNT agglomeration/aggregation but that the tissue culture medium itself contributes to this process. Most of the agglomerated p(4VP)-MWCNTs on AT2 cells (SV4–5) were easily rinsed off from the cell surface at 24 hours (Figure 2l, m, p, q; discussed below) when the experiment was terminated and the cells were rinsed before the fixation for visualization, suggesting little association with cellular tight junctions, or AT2 cell membranes, with no permanent changes in TEER.

Interaction between p(4VP)-MWCNTs and Cells

The interface between the plasma membrane and the deposited p(4VP)-MWCNTs was characterized using LM and SEM (Figure 2, Figure S2e–h) to show the interaction between MWCNTs and the cell surfaces. Control TT1 and AT2 cells formed monolayers (Figure 2f, n and Figure S2e, g). Individual 300nm p(4VP)-MWCNTs appeared to insert into the plasma membrane[28] of TT1 cells (Figure 2d–e). The individual p(4VP)-MWCNT in figure 2d has a diameter of ~30 nm, combining the expected diameter of the initial p(4VP)-MWCNT (12±4 nm) and the ~10nm gold coating during SEM sample preparation. Agglomerated p(4VP)-MWCNT were visible as black patches (Figure 2c, 2h-i) adhering to the (rinsed) surface of TT1 cells; the 300nm p(4VP)-MWCNTs formed smaller agglomerates (diameter 4.6±2.8 (±SD) μm (n=50), Figure 2c) than the 700nm p(4VP)-MWCNTs (diameter 23±11 μm (n=50), Fig. 2h). In contrast, only a few agglomerates of 300 and 700nm p(4VP)-MWCNTs, (17±8 and 20±7 (±SD, n=20) μm respectively) remained on the surface of AT2 cells; most, but not all, had disappeared, after rinsing(Figure 2l–m, p–q and SV4–5).

Pathways of p(4VP)-MWCNT Uptake and Transport

Pathways of uptake and transport of p(4VP)-MWCNT by TT1 cells were revealed using TEM, HR-TEM and CM. Similar processes of uptake and translocation across TT1 cells were observed for both 300 and 700 nm p(4VP)-MWCNTs. HR-TEM and TEM (see detail of sample preparation in methods) confirmed that individual p(4VP)-MWCNTs frequently translocated through the plasma membrane of TT1 cells and localised within the cytoplasm (Figure 3a, Figure 4a–c, respectively). The p(4VP)-MWCNTs were subsequently detected in cellular vesicles (Figure 3d, Figure 4c). We previously demonstrated, using polystyrene nanoparticles, that the uptake mechanisms in TT1 cells involve clathrin- and caveolin-mediated endocytosis.[21] In the preset study of MWCNT, individual and small aggregates of the p(4VP)-MWCNTs were found within endocytic cups at the plasma membrane (Figure 3b), whereas larger aggregates were found inside macropinosomes (Figure 3c). The p(4VP)-MWCNTs penetrated through the endo-/lysosomal membrane and were found within the cytoplasm (Figure 3d and Figure 4f–h). Vesicles containing clusters (Figure 4i) and individual p(4VP)-MWCNTs were detected at the basal side of the TT1 cells (Figure 3e–g). The p(4VP)-MWCNTs were also found at the basal side of the cells beyond tight junctions,

implying that they have crossed these junctions (TJ; black arrow in Figure 3h) *via* a paracellular route (Figure 3h, Figure 4j).

TEM and HR-TEM observations were supported using CM to study TT1 cell uptake, cell distribution and interaction with MWCNTs. The p(4VP)-MWCNTs were imaged directly using the reflectance signal, avoiding an alteration of chemical properties of the parent fMWCNTs due to fluorescent labelling.[29] In comparison to the control cell (Figure 5a, d, g), the p(4VP)-MWCNTs (Figure 5b–c, e–f) co-localised with endosomal (EEA1, Figure 5b–c) and lysosomal (LAMP1, Figure 5e–f and SV6–7) compartments, indicating endocytotic uptake mechanisms. Orthoslices taken through the yz-plane (Figure 5b1–c1, e1–f1) confirm that clusters of p(4VP)-MWCNTs (300 nm and 700nm) reached the basal side of the TT1 cells. Non-functionalised MWCNTs have been demonstrated to interact with cytoskeletal proteins in HeLa cells.[30] Morphological changes of actin in human small airway epithelial cells and human microvascular endothelial cells have also been shown after exposure to non-functionalised SWCNTs and MWCNTs.[31,32] Such interactions could disturb cell mobility and tight junction formation which could subsequently affect the TEER. Although the p(4VP)-MWCNTs (300 and 700nm) co-localised (Figure 5h–i) with the actin cytoskeleton of TT1 cells, actin morphology was not noticeably altered. Lysosomal escape of the p(4VP)-MWCNTs within TT1 cells, observed by TEM, was confirmed with live cell imaging using a pH-sensitive fluorescent dye, acridine orange (Figure S6a–h). A decrease in the fluorescent intensity of the dye relative to control indicates that p(4VP)-MWCNTs may affect the integrity of the lysosomal membranes, as reported for other MWCNTs.[33] The schematic in figure 5j summarises possible transport pathways of p(4VP)-MWCNTs across the TT1 alveolar epithelium.

Uptake of non-fMWCNTs (700nm long) and p(4VP)-MWCNTs (300nm and 700nm long) by TT1 cells were quantified at 4 and 37°C (Figure 6a) by both statistical TEM analysis and optical spectroscopy. The results indicate that the non-fMWCNT, 700nm long, exhibited no significant toxic effect (Figure S2) with significantly lower TT1 cell uptake (**$p<0.001$, $n=3$) than the 700nm long p(4VP)-MWCNTs (Figure 6a) at both temperatures. The 300nm long p(4VP)-MWCNTs exhibited significantly higher uptake (**$p<0.001$, $n=3$) than the 700nm long p(4VP)-MWCNTs under both conditions. On examining a large number ($n=3$ separate experiments with total 300 observed cells) of TT1 cells by TEM, 72% and 62% of the TT1 cells (for 300 and 700nm respectively) had internalised p(4VP)-MWCNTs at 37°C; however, the percentage was significantly reduced to 18% and 23% (**$p<0.001$, $n=3$; Figure 6a) at 4°C, indicating that the main uptake mechanism was active transport *via* endocytosis, but that passive transport also occurs. UV-vis absorbance quantified the relative percentage of p(4VP)-MWCNTs in the apical and basal chambers (Figure 6b–c), and in cell lysate (combining both adherent and internalised MWCNTs) at 24 h exposure. The majority of p(4VP)-MWCNTs (300 and 700nm) were observed in the TT1 cell lysates (70% and 58%; **$p<0.001$, $n=3$), rather than the apical chamber (20% and 26%), respectively. Up to 3% of both the 300 and 700nm p(4VP)-MWCNTs reached the basal chamber, although the concentration was saturated after 4 hours (Figure 6b–c). *In vivo* studies have suggested that for inhaled MWCNTs, 0.5–3%, could translocate into the circulation.[34–36] The relatively low concentration of p(4VP)-MWCNTs reaching the basal chamber may relate to filtration effects at the polyester support membrane; as MWCNTs become trapped at the pores (0.4

μm in diameter; Figure 7a–d) within the membrane, self-filtration will prevent further transport, leading to accumulation of MWCNTs at the membrane-cell interface (Figure 7). Considering the significant uptake of p(4VP)-MWCNTs by TT1 cells, longer term effects at 1, 3 and 7 days were considered (Figure 6d–f). Although there were no effects on dynamic cell viability over the 7-day exposure (Figure 6d), a significant continuing decrease in TEER (*$p<0.01$, **$p<0.001$, n=3) was observed (Figure 6e), correlating with a significantly increased (**$p<0.001$, n=3) p(4VP)-MWCNT uptake (Figure 6f).

In contrast to the TT1 cells, very few p(4VP)-MWCNTs were detected inside AT2 cells (Figure 8b–c, Figure 8a shows a control non-treated AT2 cell); the percentage of cell uptake observed by TEM (n=3 separate subject samples with 300 cells surveyed in total) was only 4–8% of total AT2 cells compared with 60–72% in TT1 cells (Figure 8d and SV 8–10). The rare aggregates detected within AT2 cells were mostly found within endosomal/lysosomal vesicles (Figure 8b) or occasionally within lamellar bodies (Figure 8c). The latter observation may be related to recycling of lung surfactant by AT2 cells; we recently reported that p(4VP)-MWCNTs could adsorb SP-D.[37] Adsorption of SP-A and SP-D[37,38] to p(4VP)-MWCNTs may stimulate uptake by AT2 cells following the recycling pathway. Quantification by UV/vis absorbance confirmed the TEM observations (Figure 8d). The cell lysate (including extracellular cell-adhered material) contained 13–17% of the p(4VP)-MWCNTs with the majority (~77–80%) remaining in the apical tissue culture medium compartment; no transport to the basal chamber was observed (Figure 8b). The low degree of cellular uptake and translocation was confirmed by confocal microscopic analysis (Figure 8e–g); p(4VP)-MWCNTs were not observed at the basal side of the AT2 cell monolayer (Figure 8f1, g1). No significant differences (*$p<0.01$) were measured between the 300 and 700nm p(4VP)-MWCNTs in the AT2 cell analyses. As mentioned above, the presence of PS may help to agglomerate the p(4VP)-MWCNTs, reducing cellular uptake by encapsulating the agglomerated p(4VP)-MWCNTs within the surfactant layer.

DISCUSSION

This unique study provides the first assessment of dynamic MWCNT translocation across human lung alveolar epithelium *in vitro* using a combination of statistical TEM analysis, HR-TEM, spectroscopy and confocal microscopy. These systematic techniques allowed quantification of both the proportion of alveolar epithelial cells that internalise fMWCNTs and the distribution of the fMWCNTs across the apical, cellular and basal compartments of the epithelial models. In addition, direct interactions between single p(4VP)-MWCNTs and the cell membranes were demonstrated. The zeta potential values indicated that the p(4VP)-MWCNTs likely interact with proteins in the tissue culture medium *via* an electrostatic attraction resulting in a decrease in surface charge of the p(4VP)-MWCNTs. Previous reports indicated that cationic fMWCNTs adsorbed albumin onto their surface.[30] Several pathways of uptake and translocation were identified without the need for a labelling probe, including active and passive uptake mechanisms. Others have observed polystyrene nanoparticle transport across primary rodent alveolar epithelial cells *in vitro* and highlight marked differences between rodent species regarding nanoparticle transport.[39,40] The human A549 adenocarcinoma cell line has been used as a surrogate for human AT2 cells; fMWCNT uptake by A549 cells showed internalisation by both active (endocytosis) and passive

transport (direct penetration), suggested to be due to electrostatic interaction between the hydrophilic cationic-amine moieties of fMWCNTs and the negative charge of the phospholipid cell membrane.[41] In contrast, here, primary human AT2 cells showed little inclination to internalise p(4VP)-MWCNTs. This current finding, together with our previous results, suggest that A549 may not resemble human AT2, in particular, they may not contain or release complete surfactant.[14,42,43] In fact, we suggest that the interaction of fMWCNTs with surfactant components, known to be secreted by AT2 cells *in vitro*,[14] is an important reason for the resistance of these cells to MWCNT-induced effects. Furthermore we hypothesize that spreading of the surfactant at the apical surface of type 1 cells might also modify p(4VP)-MWCNTs uptake possibly by the same mechanism but other mechanisms may also be important. We are currently investigating these hypothesis further.

Despite the lack of cell toxicity, p(4VP)-MWCNTs (Figure S2) caused a significant decrease in TEER values during exposure, paralleled with an increase in apical-basal dextran transport across the TT1 monolayer, suggesting impairment of the permeability of the TT1 cells *via* tight junction damage; however, the lack of cell death suggests the opportunity for repair. Molecular 4VP has been reported to enhance transdermal penetration of 5-fluorouracil.[44] Previous work has also shown a reduction of ZO-1 in Caco-2 gut epithelial cell monolayers exposed to carboxylic acid-functionalised single-walled carbon nanotubes after 4 and 24h exposures, while, no change was observed in cells exposed to polyhydroxy fullerene.[45] The shape and surface functionalization of carbon-based nanomaterials are key parameters and mechanisms involved in the reversible modulation of tight junctions and the inhibition of the P-glycoprotein efflux system.[45] More generally, cationic dendrimer nanoparticles encourage paracellular transport by opening the tight junctions *via* a dynamin-dependent uptake mechanism.[46] It is not yet clear if a similar mechanism may apply to these p(4VP)-MWCNTs, which do not exhibit a positive charge in tissue culture medium. The control experiment using p(4VP) at a concentration of 1μg/ml, equivalent to that introduced *via* p(4VP)-MWCNT samples, showed negligible toxicity (Figure S2a–d) and non-significant changes in TEER following 24h exposure (Figure 1a–b). Therefore, the decrease in TEER induced by the p(4VP)-MWCNTs most likely relates to the effect of the MWCNTs. The results of the degree of fMWCNT agglomerates/aggregates (Figure 2, Figure S5 and SV2–5) also helps us to interpret the key parameter that may affect TEER in this study. In all the conditions studied, the 700nm fMWCNTs appear to significantly agglomerate/aggregate more than the 300nm fMWCNTs (Figure S5e, ***$p<0.001$, $n=3$). The 700nm long fMWCNT also form larger aggregates (diameter 23±11(±SD) μm, Figure 2c) than the 700nm long p(4VP)-MWCNTs (diameter 4.6±2.8μm). Conversely, the bar graph in figure S5, together with figure 2 in the manuscript, indicate that the 300nm long fMWCNT agglomerates/aggregates are quantitatively less and much smaller. Concentrating on the TT1 cell data (Figure S5e and Figure 1–2), one could hypothesise that the 300nm long fMWCNTs, either as dispersed MWCNTs (78% of exposed fMWCNTs) or as small agglomerates/aggregates (22%), has greater access to the cell surface and cell-cell junctions than the larger 700nm agglomerates/aggregates (69%) and dispersed fMWCNTs (31%) and therefore causes more cell barrier disruption and is more readily internalised by the TT1 cells. The confocal results (Figure 5h–i) show the co-localisation between the aggregated fMWCNTs and actin filaments which are involved in tight junction formation suggesting

that the p(4VP)-MWCNT aggregates may also induce TEER reduction. Therefore, the higher impact on TEER reduction of the 300nm long MWCNT could be due to the significantly greater numbers of individualised 300nm fMWCNTs in the system compared with 700nm long MWCNTs.

Functionalisation the MWCNTs with p(4VP) significantly enhanced cell uptake (**$p<0.001$, $n=3$) and increased stability of fMWCNT suspension. The amount of TT1 cell uptake of shorter 300nm p(4VP)-MWCNTs was significantly greater (**$p<0.001$, $n=3$) compared to the 700 nm p(4VP)-MWCNTs, and correlated with significantly altered permeability of the TT1 cells. In contrast, the full recovery of TEER value in AT2 cells, exposed to both types of p(4VP)-MWCNTs, may be related to the much lower cellular uptake, the stronger tight junctions, and the protective effect of AT2 cell secretions. The finding that p(4VP)-MWCNT aggregates were observed on AT2 cell monolayer, but that most of the aggregates were removed following the rinsing process for visualisation, suggests that the cell secretions could activate MWCNT aggregation and these aggregates and any remaining individual MWCNTs could be trapped within the PS layer secreted by AT2 cells. Therefore, the MWCNTs could not reach the cell membrane or cell-cell junctions. Thus, the effect of p(4VP)-MWCNTs on TEER of AT2 cells, possibly due to changes in surfactant behavior and the variation in components of the secretions, was reversible. We recently demonstrated that TT1 cells exhibited higher percentage (>95%) of internalised 50 and 100nm polystyrene latex nanoparticle (NP) than that of the AT2 cells (<5%), and the uptake of cationic-NPs was higher than that of the anionic- and neutral-NPs.[21] Marchetti *et al*. have reported that the p(4VP)-MWCNTs adsorbed SP-D from human AT2 secretions.[37] Our observations also suggest that the interaction between AT2 secretions and p(4VP)-MWCNTs might induce agglomeration or aggregation of p(4VP)-MWCNTs, and it may be that, *in vivo*, together with adsorption of SP-D onto MWCNTs, this process could facilitate macrophage clearance.

This comparative study of alveolar monocultures does not address the effects of the co-existence *in vivo* of type 1 and type 2 alveolar epithelial cells in close proximity to each other *in situ*. An *in vitro* model to mimic this situation and therefore examine how simultaneous treatment of mixed epithelial cell models to fMWCNTs would provide further information, taking into account the physiological effects of adjacent type 1 and type 2 cell communication, as well as the influence of type 2 cell secretions on the response of the alveolar epithelial membrane to fMWCNTs treatment. However, the fundamental information of the bioreactivity, uptake, and transport of fMWCNTs through each individual cell type can generate a better understanding in the co-culture model and *in vivo*. Importantly, the current study clearly demonstrates how the differences between TT1 and AT2 cells in cell morphology and function impact on the magnitude and profile of their response to p(4VP)-MWCNTs. Thus, we are currently developing co-cultures of alveolar type 1 and type 2 cells to further understand the impact of nanoparticle drug delivery to the alveolar epithelial interface.

CONCLUSION

This current study clearly demonstrated that the p(4VP)-MWCNTs showed no effect on cell viability but they can cause alteration in TEER value depending on cell types, duration of

exposure and length of p(4VP)-MWCNTs. The impairment of the integrity of the alveolar membrane could have undesirable effects, for example by increasing susceptibility to respiratory infection,[47] and unwanted delivery to the systemic circulation might affect blood clotting, and increase unwanted access other organs, possibly inducing adverse health effects[48,49] However, a moderate change in barrier permeability might be desirable to enhance translocation of highly functionalised nanodrugs to the systemic circulation for targeted drug delivery, and might be quite useful, particularly if reversible. The stark differences shown in this study comparing the two human alveolar epithelial cell types, illustrate how the *in vivo* function of a cell will significantly impact on its interaction with, and response to, exogenous challenges. Thus, AT2 cells generate strong tight junctions and release surfactant which modify the behaviour of nanomaterials which deposit at this interface, whilst the AT1 cell ostensibly would be the major cell for targeted drug delivery where translocation to other lung compartments, or systemically, is desirable. A combination of statistical TEM analysis, HR-TEM, spectroscopy and confocal microscopy allowed quantification of both fMWCNT uptake and transport across epithelium monolayer without using labelling probe. The direct interactions between single p(4VP)-MWCNTs and the cell membranes can also be elucidated.

METHODS

Preparation of Monoculture Model of TT1 Cells

The TT1 cells were created from primary human alveolar epithelial type 2 cells (AT2) isolated from the healthy region of tissues as previously described which shows the same characteristic and phenotype as AT1 *in vivo*.[12] TT1 cells were routinely characterised by immunofluorescent staining of antibodies against RAGE and caveolin-1.[12] Immortalized AT1-like human alveolar epithelial cells (TT1[12]) were cultured in DCCM 1 medium (Cadama, UK) supplemented with a mixture of 100U/ 100U/ 2mM of Penicillin/ Streptomycin/L-Glutamin (SPG; Invitrogen, UK) and 10% newborn calf serum (NCS; Invitrogen, UK). Cells were seeded at 5×10^5 cells/well on 12 well Transwell® plate polyester membrane support with pore size of 0.4μm (Corning, UK) at 37 °C, 5 % CO_2 and the fresh medium was replaced every two days. Cells were grown for 1 week and at 24h before the exposure, the complete medium was replaced by DCCM1 serum free medium.

Preparation of Monoculture Model of Primary Human Alveolar Epithelial Cells (AT2)

AT2 cell isolation from tissues was performed as previously described.[14] The tissue used in this study was surplus tissue obtained following resection for lung carcinoma and the written informed consent was obtained for all samples. The study was carried out with the approval of the Royal Brompton and Harefield Ethical Committee (Ref: 08/H0708/73). Although the tissue were obtained from resection for lung carcinoma diagnosis, only lung tissue with normal appearance was taken from the pleural border, distal to the tumor, for use in this study. The tissue was rinsed and, then, repeatedly perfused with 0.15M sodium chloride solution (NaCl) to remove excess blood and virtually free from leukocytes ($<10^4$/ml). The tissue was next fully inflated with trypsin (0.25% in HBSS; Sigma-Aldrich, UK) and incubated at 37°C for 45min. The tissue was minced finely in newborn calf serum (NCS; Invitrogen, UK). A 1:1 ratio of the minced tissue and DNase I (Sigma-Aldrich, UK; 250

mg/ml in Hanks balance solution (HBSS)) were mixed and shaken by hand for 5 min. This suspension was filtered through 400-then 40-μm mesh, respectively. The filtrate was centrifuged to collect the isolated cells. The cell pellet was suspended in DCCM1 containing 100 mg/ml DNase I, and plated into a T-75 flask to allow adhesion of contaminating leukocytes and other cells (at 37°C for 2 h). The supernatant containing nonadherent, AT2 cell–enriched cells was centrifuged at 1300xg for 10 min. The pellet was resuspended in DCCM1 with a mixture of 100U/ 100U/ 2mM of PSG and 10% NCS and plated into a T-75 flask at 37°C for 1–2 h to allow fibroblastic cells to adhere. The nonadherent AT2 cell–enriched supernatant was removed from the flask and collected by centrifugation at 1300xg for 10 min, and the pellet was resuspended in DCCM1 medium (Cadama, UK) containing 10% NCS and 1% PSG, and seeded at 2×10^6 cells/well on 1% type I collagen (PureCol, Netherland) pre-coated Transwell® plates (Corning, UK) at 37 °C, 5 % CO_2. After 48 h, cells were confluent and had a purity of >95%. The cells were thoroughly characterised using electron microscopy illustrating their cuboidal morphology, lamellar bodies, tight junctions and microvilli. They were also stained positively for the ATII cell marker alkaline phosphatase and expressed surfactant proteins A and C. These AT2 cell could maintain their phenotype for up to 6 days,[14] the cells were used within 48h following the confluence. Cells were then serum starved for 24 h before the MWCNT-exposure. Overall 6 subject samples were used including: 2 non-smokers, 3 ex-smokers and 1 current smoker. Six separated experiments were performed using AT2 isolated from six different tissues with 3–5 replicate readout on each experiment. There was a wider range in the data in the experiments performed on the AT2 cells, compared with the data obtained from the TT1 cells (Figure 1 and Figure S2). We did not observe a striking different between the population of non-smokers, current smokers and ex-smokers as the number of subjects in each population was low. It is clear that the profile of the response to p(4VP)-MWCNTs was the similar between difference subject samples.

Exposure of Cells to p(4VP)-MWCNTs

TT1 cells were routinely seeded and cultured into each well of a 12-well transwell plate, in DCCM1 (Cadama, UK), 10% new born calf serum (Invitrogen, UK) and 10% Penstrep (Invitrogen, UK). AT2 cells were seeded at the same density on the collagen coated plate, as mentioned previously. At confluence, 24 h prior to non-fMWCNTs (p-MWCNTs)/p(4VP)-MWCNTs exposure, the medium was replaced with serum-free DCCM1. The cells were exposed to 1–30 μg/ml of non-fMWCNTs/p(4VP)-MWCNTs for 24h at 37°C. For the longer exposure, the medium within basal chamber was changed every two days. For the TT1 cells, three replicate experiments (TT1) were conducted. Six replicate experiments (AT2) were performed with the AT2 cells respectively.

Cell Viability (WST)

Cell viability of cell exposed to non-fMWCNTs (p-MWCNTs), 300 and 700nm, long, p(4VP)-MWCNTs and p(4VP) were analysed using the Cell Proliferation Reagent WST-1 (Roche, UK). In brief, cells were exposed to p(4VP)-MWCNTs, 1–30μg/ml, for 24h. The cells were rinsed with phosphate buffer solution (PBS; x3) and incubated with the medium contained tetrazolium salt of WST-1 (dilution 1:10 from stock) for 1h. The medium was collected and measured the absorbance at 450nm. The percent cell viability was calculated

according to the control non-treated cells and data were presented as percent viability in proportional to that of the non-treated cells (n=3 (number of experiments on TT1) and n=6 (number of subject samples and experiments on AT2)) with error bars showing standard deviation (SD).

Lactate Dehydrogenase Assay (LDH)

After 24h exposure, the conditioned medium was collected and centrifuged at 14,000 g for 20 min to remove the cell debris and residual p(4VP)-MWCNTs/non-fMWCNTs (p-MWCNTs). LDH was analyzed using the Cytotoxicity Detection kit PLUS (LDH; Roche, UK). For the control and substance control, a known concentration of LDH standard (0.05 U/ml) was incubated with a sample of DCCM1 medium, with or without increasing concentrations of the p(4VP)-MWCNTs, non-fMWCNTs and p(4VP) and the assay performed in an identical manner. There was no significant interference of the p(4VP)-MWCNTs/non-fMWCNTs, which were removed by centrifugation prior to reading the optical density (number of experiments, n=3 (TT1) and n=6 (AT2)).

Release of Inflammatory Mediators (IL-6 and IL-8)

The release of inflammatory mediators interleukin 6 and 8 (IL-6 and IL-8) into the 24h-exposure media were measured using sandwich enzyme-linked immunosorbent assays (ELISA). The assays were performed using DuoSet® antibody kits (R&D systems, USA). The TT1 and AT2 cells were exposed to 300 and 700nm p(4VP)-MWCNTs for 24h; the exposed media were then collected and centrifuged at 12,000xg to remove the MWCNTs before performing assay. The data were collected by reading optical absorption at a wavelength of 450nm using a Thermomax microplate reader (MTX Lab Systems, USA). For TT1 cells, three replicate experiments with 3 readouts per experiment, were performed (n=3). For AT2 cells six replicate experiment, 3 readouts per experiment, were carried out using cells isolated from six different subjects samples (n=6).

Transepithelial Electrical Resistance (TEER) Measurement

The TEER values of cell monolayers were monitored before the exposure and at 1, 2, 4, 8, 10, 16 and 24h during the exposure using Millicell®-ERS (Millipore, UK). During 7d exposures the TEER values were measured at 0, 24, 72h, and 7d. The electrode was rinsed and wiped clean every time before measuring TEER in each well. Three separate experiments were performed (n=3 (TT1), and n=6 for AT2).

Immunofluorescent Staining for Confocal Microscopy (CM)

After the exposure, the TT1 and AT2 cells were rinsed twice with PBS, fixed with 4% paraformaldehyde in PBS, and permeabilised with 0.1% triton X-100 with 0.5% FCS in PBS. Samples were then rinsed again with PBS three times for 5 min and incubated with 1% BSA in PBS for 40 min before incubating with primary antibody of EEA1, LAMP1, actin or ZO-1 (1:100; Rabbit polyconal IgG against EEA1, LAMP1 or ZO-1 from Invitrogen, UK) in 1% BSA overnight at 4°C in dark. The next day cells were rinsed (x3) and incubated with secondary antibody (1:200; Alex Fluor®594 - goat anti rabbit IgG from Invitrogen, UK) in 1% BSA in PBS for 1h at room temperature. Cells were then counter stained with DAPI and

rinsed with PBS. Finally, membrane were cut and mounted onto the microscope slides using Prolong® Gold (Invitrogen, UK), kept at 4–8°C before imaging using the laser scanning confocal microscopy (Ziess LSM-510 inverted confocal microscopy, Germany). Three separate experiments were carried out with 50 cells surveyed (in total 150 cells were surveyed).

Live Cell Imaging and Lysosomal Escape of p(4VP)-MWCNTs (Light Microscopy and Confocal Microscopy) in TT1 cells

For normal live cell imaging, after the p(4VP)-MWCNT exposure the cells were rinsed with PBS (x3) and the cell were transferred to live cell imaging chamber that maintained the temperature at 37°C with 5%CO_2 and 95% O_2. The cell were imaged using (Leica SP2 inverted fluorescent microscopy, Germany) using optical zoom x10 and x20. To observe lysosomal escape of MWCNTs, after the p(4VP)-MWCNT exposure, the cells were incubated with acridine orange (AO; Invitrogen, UK), pH sensitive dye, for 20 min. AO is a pH sensitive dye that normally accumulate in acidic compartment of lysosomes within the cells and exhibit a high intensity of red fluorescent at acidic pH, when it is released from lysosome the fluorescent intensity will rapidly reduce within a non-acidic environment. The cells were washed with PBS twice before they were then observed without fixing under the confocal microscope (Leica SP5 MP inverted confocal microscopy, Germany). Cells were maintained with 5% CO_2 and 95% O_2 in the live cell imaging chamber with heated stated setting 37°C. The reduction of fluorescent intensity of the AO was analysed using ImageJ (FIJI) and Velocity® software version 6.3.1 (PerkinElmer Inc., UK). Experiment were carried out in triplicate (n=3).

Determination of the Degree of p(4VP)-MWCNT Agglomeration/Aggregation Using Light Microscopy and Spectroscopy

To investigate the degree of agglomeration/aggregation, 15μg/ml of 300nm and 700nm, long, p(4VP)-MWCNTs were incubated without/with TT1 or AT2 monocultures in a 12 well-plate for 24 h for 24h at 37°C with 5% CO_2. In cell-exposure system, the monoculture of TT1 or AT2 cells were incubated to 15μg/ml of 300nm/700nm, in length, p(4VP)-MWCNTs as descripted above in ‘Exposure of cell to p(4VP)-MWCNTs’ section. In the cell-free exposure system, TT1 and AT2 were, first, exposed to serum-free DCCM1 medium for 24h at 37°C with 5% CO_2 ; this 24h-exposed medium was collected and treated as ‘condition medium’. The fMWCNTs were subsequently incubated with the ‘conditioned medium’ in a 12 well-plate for another 24 h at 37°C with 5% CO_2. Control studies were performed without cells by incubating the fMWCNTs with fresh serum-free DCCM1 medium at 37°C with 5% CO_2 for 24h to analyse the effect of anything within the DCCM1 culture medium. Following 24h the media were carefully collected without disturbing the sedimented MWCNTs which were then collected by rinsing the well with 1ml PBS. The concentrations of the MWCNTs within the rinsed solutions and the collected media were measured using UV-vis spectrometer (Lambda 950, Perkin Elmer) at a wavelength of 800nm. For live cell imaging the cell were transferred to live cell imaging chamber that maintained the temperature at 37°C with 5%CO_2 and 95% O_2. The images of the exposed cells before and after the rinsing were taken; the rinsing process (video) was also captured (Leica SP2 inverted fluorescent microscopy, Germany) using optical zoom x10 and x20 to

show the protective effect of the AT2 cell secretions. Experiments were performed in triplicate (n=3).

Scanning Electron Microscopy (SEM)

After the exposure to p(4VP)-MWCNTs, TT1 and AT2 cells grown on the transwell membranes were rinsed several times to remove the excess particles and final rinsed with 0.1M HEPES pH7.2 before they were fixed in 2.5% glutaraldehyde in 0.1 M cacodylate buffer for 2 h at 4°C. Subsequent dehydration was performed using a graded series of ethanol (50%, 70%, 90% and dry 100% ethanol) for 15min (x3 each) in each solution. Samples were then dried by evaporation immersion in hexamethyldisilazane for 2 min and left in a fume cupboard for 2 h. Dried samples were attached to aluminium stubs, gold coated, and examined under SEM, at an accelerating voltage of 5kV, with the InLens detector at 50,000–150,000x magnification (LEO Gemini 1525 FEG-SEM, Germany). For each sample, 50 cells were randomly selected to survey and experiments were performed in triplicate (n=3 with 150 cells surveyed in total).

Transmission Electron Microscopy (TEM)

Following exposure to p(4VP)-MWCNTs, TT1 and AT2 cells were rinsed twice with 0.1M HEPES pH7.2 and fixed with 2.5% glutaraldehyde in 0.1M cacodylate buffer for 2h and then rinsed with sodium cacodylate buffer. Samples were then post-fixed in 1% osmium tetroxide for 30min and dehydrated using a graded series of ethanol (50%, 70%, 90% and dry 100% ethanol) for 15min (x3) in each solution. Samples were incubated with 25, 50, 75 and 100% in ethanol of Aradite® for 20min (x3) each and the fresh 100% Aradite® was added and incubated at 60°C for 24h. The embedded samples were sectioned using a 35 degree diamond knife (DiATOME) to a thickness of 50–100nm. The sections were observed in a JEOL 2000 transmission electron microscope operated at an accelerating voltage of 80 kV to increase contrast from cell organelles. Multiple cells (n=3 for TT1 and AT2 cells, with 300 cells surveyed in total) from three cell exposures were surveyed by TEM (JEOL 2000FX, Japan) operated at 80 KV with an objective aperture.

High Resolution Bright-Field Transmission Microscopy (HR-TEM)

Cell monolayer of TT1 and AT2 cells were fixed and processed in the same way as normal TEM samples (previously described in the method section with the main text). High resolution bright-field TEM (HR-TEM) imaging was carried out on a C_s-aberration-corrected FEI TitanTM 80–300 scanning/transmission electron microscope (S/TEM) operated at 80 kV. HRTEM images were captured on a Gatan 2kx2k US1000 CCD camera (Thermis (EFI, Oregon, USA)) with a 100 μm size objective aperture inserted. The accelerating voltage used in this study was 80 kV, which is below the critical threshold energy predicted for severe knock-on damage in MWCNT.[50]

Quantification of the Uptake and Transport of the p(4VP)-MWCNTs by Cells Using UV–Vis Spectroscopy and Dosage Calculation

Following our studies, the cells were exposed to 15μg/ml (6.7μg/cm^2) of 300 and 700nm p(4VP)-MWCNTs for up to 24h, the minimum dose that can be detected using UV-vis

spectroscopy. Dynamic uptake and transport of the p(4VP)-MWCNTs were monitored by measuring the UV absorbances of the cell lysate and the medium collected from apical and basal chamber using a UV-vis spectrometer (Lambda 950, Perkin Elmer) at a wavelength of 800nm at different time intervals up to 24h. The concentrations of grafted MWCNTs were determined from UV absorbance according to the application of the Beer-Lambert law as described in p(4VP)-MWCNT synthesis section. Briefly, cell culture medium collected from apical and basal chambers of the transwell plate (cell free samples) were bath sonicated for 30 min (45kHz, 80W, VWR International) before the measuring. For cell lysate, the cells were lysed and solubilised with 200μl of CelLytic M cell lysis reagent (Sigma, UK) and diluted with 0.1% SDS to help to solubilized all cell debris to reach total volume of 1ml. The samples were finally bath sonicated for 30minutes (45kHz, 80W, VWR International) before the measuring. The control of lysis buffer in 0.1% SDS was used as blank for background subtraction of cell-free samples. For cell lysate samples, the control of non-treated cell lysate solution was used as blank. Experiments were performed in triplicate (n=3) for TT1the cells and 5 separate experiments (from 5 sample subjects) were performed for the AT2 cells (n=5).

Quantification of the Uptake and Transport of the p(4VP)-MWCNTs by Cells Using TEM

To quantify the percentage of cell uptake statistical TEM analysis was employed. Following exposure to non-fMWCNTs (p-MWCNTs) and p(4VP)-MWCNTs, TT1 and AT2 cells were rinsed twice with 0.1M HEPES pH7.2 and fixed with 2.5% glutaraldehyde in 0.1M cacodylate buffer for 2h and processed for TEM sample preparation as described in TEM section. Active and passive uptake of p-MWCNT and p(4VP)-MWCNTs were also investigated by incubating the cells with p-MWCNTs/p(4VP)-MWCNTs at 4°C and 37°C for 4h. The cells were fixed and processed (described above) for TEM analysis as previously described.[51] Three sections from three embedded capsules (n=3) were viewed per sample; 100 cells were randomly surveyed in each section (300 cells were surveyed in total). The percentage of MWCNT internalized cells was calculated in proportion to the total cell count and data were presented as mean±SD (n=3). This sampling profile is much greater than that performed in much of the literature on MWCNT cell interactions. It would not be feasible to increase the sample size for imaging experiments as this work is extremely time demanding and expensive to conduct, particularly since the results were the same for all 3 subjects. Instead we have correlated between microscopy analyses and quantitative UV-Vis spectroscopy data to increase the statistical significance of our findings. To our knowledge this is the first study which has used a quantitative approach to supplement and validate the issue of cell sampling using TEM only; this further emphasis the novelty of our work.

Data Analysis

The data were first tested for a normal distribution using D'Agostino-Pearson normality test or Shapiro-Wilk normality test (α=0.05, p>0.05) and the data exhibited a normal distribution (Graph Pad Prism 5.0). For viability studies, the difference between the doses of 4VP-MWNTs on cell viability (WST and LDH) within one cell type was analysed using one-way ANOVA with a Post-Hoc (Bonferroni) test to confirm differences. The same analysis was applied to determine the difference between cellular TEER values at different time points with, and without, 4VP/300m/700nm 4VP-MWCNTs. The difference between TEER

values/dextran permeability/ECIS at different time points on one cell type, non-treated or treated, was also analysed using one-way ANOVA.

The difference in viability between treatment (non-treated, 4VP, 300nm (4VP)-MWCNT and 700nm (4VP)-MWCNTs) at different doses (two-variables) within one cell type were analysed using in two-way ANOVA with Post-Hoc test (Bonferroni). A similar analysis was applied to see the difference in TEER values with different treatments (non-treated, 4VP, 300nm and 700nm (4VP)-MWCNTs) and at different time points within one cell type. Two-way ANOVA was also applied other experiments including acridine orange leakage (variables are time and length of the MWCNTs), (4VP)-MWCNT uptake (variables are temperature and length of the MWCNT/time and length MWCNT) and D/G ratio (variables are time and length of MWCNT). Comparison the uptake between cell types was performed using an unpaired t-test. All statistical analysis was performed using Graph Pad Prism 5.0 and SPSS 17. Differences were considered significant at *$p<0.01$ and **$p<0.001$. Values are shown as mean ± SD.

Supplementary Material

Refer to Web version on PubMed Central for supplementary material.

ACKNOWLEDGMENT

This study was supported by an award from the Leverhulme Trust (project no. F/07058/BT), UK and by the European Research Council (project no. 257182) to AEP. This work was also supported by NIEHS (project no. U19ES019536) to TDT and the NIHR Respiratory Disease Biomedical Research Unit at the Royal Brompton and Harefield NHS Foundation Trust and Imperial College London.

Funding Sources

This work was sponsored by Leverhulme Trust (UK; project no. F/07058/BT), European Research Council (project no. 257182), NIEHS (project no. U19ES019536) and NIHR Respiratory Disease Biomedical Research Unit at the Royal Brompton and Harefield NHS Foundation Trust and Imperial College London.

ABBREVIATIONS

CNT	Carbon nanotube
short-fMWCNTs	short functionalised multi-walled carbon nanotube
TEER	trans epithelial electrical resistance
PS	pulmonary surfactant
AT1	human alveolar epithelial type 1 cells
TT1	immortalised human alveolar epithelial type 1 cells
AT2	primary human alveolar type 2 cells
p(4VP)-MWCNT	multi-wall carbon nanotube grafted with 4-vinyl-pyridine
SEM	scanning electron microscopy

TEM	transmission electron microscopy
LM	light microscopy
CM	laser scanning confocal microscopy
SPG	penicillin/streptomycin/L-glutamin
NCS	newborn calf serum
DCCM1	Defined Cell Culture Media
PS	surfactant proteins
SP-A	surfactant protein A
SP-D	surfactant protein D
PE	polyester membrane support
AO	acridine orange
PBS	phosphate buffer saline solution
SI	supporting information
SV	supporting video

REFERENCES

1. Spitalsky Z; Tasis D; Papagelis K and Galiotis C Carbon Nanotube-Polymer Composites: Chemistry, Processing, Mechanical and Electrical Properties. Prog. Polym. Sci 2009, 35, 357–401.
2. Bates K and Kostarelos K Carbon Nanotubes as Vectors for Gene Therapy: Past Achievements, Present Challenges and Future Goals. Adv. Drug Deliv. Rev 2013, 65, 2023–2033. [PubMed: 24184373]
3. De Volder MF; Tawfick SH; Baughman RH and Hart AJ Carbon Nanotubes: Present and Future Commercial Applications. Science 2013, 339, 535–539. [PubMed: 23372006]
4. Castranova V; Schulte PA and Zumwalde RD Occupational Nanosafety Considerations for Carbon Nanotubes and Carbon Nanofibers. Acc. Chem. Res 2013, 46, 642–649. [PubMed: 23210709]
5. Morimoto Y; Horie M; Kobayashi N; Shinohara N and Shimada M Inhalation Toxicity Assessment of Carbon-Based Nanoparticles. Acc. Chem. Res 2013, 46, 770–781. [PubMed: 22574947]
6. Tang S; Tang Y; Zhong L; Murat K; Asan G; Yu J; Jian R; Wang C and Zhou P Short- and Long-Term Toxicities of Multi-Walled Carbon Nanotubes in vivo and in vitro. J. Appl. Toxicol 2012, 32, 900–912. [PubMed: 22760929]
7. Liu Y; Zhao Y; Sun B and Chen C Understanding the Toxicity of Carbon Nanotubes. Acc. Chem. Res 2013, 46, 702–713. [PubMed: 22999420]
8. Chen S; Hu S; Smith EF; Ruenraroengsak P; Thorley AJ; Menzel R; Goode AE; Ryan MP; Tetley TD; Porter AE and Shaffer MS Aqueous Cationic, Anionic and Non-Ionic Multi-Walled Carbon Nanotubes, Functionalised with Minimal Framework Damage, for Biomedical Application. Biomaterials 2014, 35, 4729–4738. [PubMed: 24631251]
9. Murphy FA; Schinwald A; Poland CA and Donaldson K The Mechanism of Pleural Inflammation by Long Carbon Nanotubes: Interaction of Long Fibres with Macrophages Stimulates them to Amplify Pro-Inflammatory Responses in Mesothelial Cells. Part. Fibre. Toxicol 2012, 9, 8. [PubMed: 22472194]

10. Crapo JD; Young SL; Fram EK; Pinkerton KE; Barry BE and Crapo RO Morphometric Characteristics of Cells in the Alveolar Region of Mammalian Lungs. Am. Rev. Respir. Dis 1983, 128, S42–S46. [PubMed: 6881707]
11. Ng AW; Bidani A and Heming TA Innate Host Defense of the Lung: Effects of Lung-Lining Fluid pH, Lung 2004, 182, 297–317. [PubMed: 15742242]
12. Kemp SJ; Thorley AJ; Gorelik J; Seckl MJ; O'Hare MJ; Arcaro A; Korchev Y; Goldstraw P and Tetley TD Immortalization of Human Alveolar Epithelial Cells to Investigate Nanoparticle Uptake. Cell Mol. Biol 2008, 39, 591–597.
13. Sun H; Quan Y; Yan Q;Peng X; Mao Z; Wetsel RA and Wang D Isolation and Characterization of Alveolar Epithelial Type II Cells Derived from Mouse Embryonic Stem Cells, Tissue Eng Part C. Methods 2014, 20, 464–472. [PubMed: 24102479]
14. Witherden IR and Tetley TD Isolation and Culture of Human Alveolar Type II Pneumocytes, Methods Mol. Med 2001, 56, 137–146. [PubMed: 21336897]
15. Barkauskas CE; Cronce MJ; Rackley CR; Bowie EJ; Keene DR; Stripp BR; Randell SH; Noble PW and Hogan BL Type 2 Alveolar Cells are Stem Cells in Adult Lung. J. Clin. Invest 2013, 123, 3025–3036. [PubMed: 23921127]
16. Wong BS; Yoong SL; Jagusiak A; Panczyk T; Ho HK; Ang WH and Pastorin G Carbon Nanotubes for Delivery of Small Molecule Drugs. Adv. Drug Deliv. Rev 2013, 65, 1964. [PubMed: 23954402]
17. Foldvari M and Bagonluri M Carbon Nanotubes as Functional Excipients for Nanomedicines: II. Drug Delivery and Biocompatibility Issues. Nanomedicine 2008, 4, 183–200. [PubMed: 18550450]
18. Menzel R; Tran CL; Menner A; Kay CWM; Bismarck A and Shaffer MSP A Versatile, Solvent-Free Methodology for the Functionalisation of Carbon Nanotubes. Chem. Sci 2010, 1, 603–608.
19. Hong S; Kim M; Hong CK; Jung D and Shim SE Encapsulation of Multi-Walled Carbon Nanotubes by Poly(4-vinylpyridine) and its Dispersion Stability in Various Solvent Media. Synthetic Met 2008, 158, 900–907.
20. Elbert KJ; Schafer UF; Schafers HJ; Kim KJ; Lee VH and Lehr CM Monolayers of Human Alveolar Epithelial Cells in Primary Culture for Pulmonary Absorption and Transport Studies. Pharm. Res 1999, 16, 601–608. [PubMed: 10349999]
21. Thorley AJ; Ruenraroengsak P; Potter TE and Tetley TD Critical Determinants of Uptake and Translocation of Nanoparticles by the Human Pulmonary Alveolar Epithelium. ACS Nano 2014, 8, 11778–11779. [PubMed: 25360809]
22. Gasser M; Rothen-Rutishauser B; Krug HF; Gehr P; Nelle M; Yan B and Wick P The Adsorption of Biomolecules to Multi-Walled Carbon Nanotubes is Influenced by Both Pulmonary Surfactant Lipids and Surface Chemistry. J. Nanobiotechnology 2010, 8, 31. [PubMed: 21159192]
23. Kapralov AA; Feng WH; Amoscato AA; Yanamala N; Balasubramanian K; Winnica DE; Kisin ER; Kotchey GP; Gou P; Sparvero LJ; Ray P; Mallampalli RK; Klein-Seetharaman J; Fadeel B; Star A; Shvedova AA and Kagan VE Adsorption of Surfactant Lipids by Single-Walled Carbon Nanotubes in Mouse Lung upon Pharyngeal Aspiration. ACS Nano 2012, 6, 4147–4156. [PubMed: 22463369]
24. Hu G; Jiao B; Shi X; Valle RP; Fan Q and Zuo YY Physicochemical Properties of Nanoparticles Regulate Translocation across Pulmonary Surfactant Monolayer and Formation of Lipoprotein Corona. ACS Nano 2013, 7, 10525–10533. [PubMed: 24266809]
25. Kendall M; Ding P; Mackay RM; Deb R; McKenzie Z; Kendall K; Madsen J and Clark H Surfactant Protein D (SP-D) Alters Cellular Uptake of Particles and Nanoparticles. Nanotoxicology 2013, 7, 963–973. [PubMed: 22551051]
26. Kendall M; Tetley TD; Wigzell E; Hutton B; Nieuwenhuijsen M and Luckham P Lung Lining Liquid Modifies PM (2.5) in Favor of Particle Aggregation: a Protective Mechanism. Am. J. Physiol Lung Cell Mol. Physiol 2002, 282, L109–L114. [PubMed: 11741822]
27. Kendall M; Ding P and Kendall K Particle and Nanoparticle Interactions with Fibrinogen: the Importance of Aggregation in Nanotoxicology. Nanotoxicology 2011, 5, 55–65. [PubMed: 21417688]

28. Baoukina S; Monticelli L and Tieleman DP Interaction of Pristine and Functionalized Carbon Nanotubes with Lipid Membranes. J. Phys. Chem. B 2013, 117, 12113–12123 (2013). [PubMed: 24024494]
29. Meng L; Fu C and Lu Q Advanced Technology for Functionalization of Carbon Nanotubes. Prog. Nat. Sci 2009, 19, 801–810.
30. Cai X; Ramalingam R; Wong HS; Cheng J; Ajuh P; Cheng SH and Lam YW Characterization of Carbon Nanotube Protein Corona by Using Quantitative Proteomics. Nanomedicine 2013, 9, 583–593. [PubMed: 23117048]
31. Holt BD; Short PA; Rape AD; Wang YL; Islam MF and Dahl KN Carbon Nanotubes Reorganize Actin Structures in Cells and ex vivo. ACS Nano 2010, 4, 4872–4878. [PubMed: 20669976]
32. Snyder-Talkington BN; Schwegler-Berry D; Castranova V; Qian Y and Guo NL Multi-Walled Carbon Nanotubes Induce Human Microvascular Endothelial Cellular Effects in an Alveolar-Capillary Co-Culture with Small Airway Epithelial Cells. Part. Fibre. Toxicol 2013, 10, 35. [PubMed: 23903001]
33. Mu Q; Broughton DL and Yan B Endosomal Leakage and Nuclear Translocation of Multiwalled Carbon Nanotubes: Developing a Model for Cell Uptake. Nano. Lett 2009, 9, 4370–4375. [PubMed: 19902917]
34. Reddy AR; Krishna DR; Reddy YN and Himabindu V Translocation and Extra Pulmonary Toxicities of Multi Wall Carbon Nanotubes in Rats. Toxicol. Mech. Methods 2010, 20, 267. [PubMed: 20482408]
35. Czarny B; Georgin D; Berthon F; Plastow G; Pinault M; Patriarche G; Thuleau A; L'Hermite MM; Taran F and Dive V Carbon Nanotube Translocation to Distant Organs After Pulmonary Exposure: Insights from in situ (14)C-Radiolabeling and Tissue Radioimaging. ACS Nano2014, 8, 5715. [PubMed: 24853551]
36. Stapleton PA; Minarchick VC; Cumpston AM; McKinney W; Chen BT; Sager TM; Frazer DG; Mercer RR; Scabilloni J; Andrew ME; Castranova V and Nurkiewicz TR Impairment of Coronary Arteriolar Endothelium-Dependent Dilation After Multi-Walled Carbon Nanotube Inhalation: a Time-Course Study. Int. J. Mol. Sci 2012, 13, 13781–13803. [PubMed: 23203034]
37. Marchetti M; Shaffer MS; Zambianchi M Chen S; Superti F; Schwander S; Gow A; Zhang JJ; Chung KF; Ryan MP; Porter AE and Tetley TD Adsorption of Surfactant Protein D from Human Respiratory Secretions by Carbon Nanotubes and Polystyrene Nanoparticles Depends on Nanomaterial Surface Modification and Size. Philos. Trans. R. Soc. Lond B Biol. Sci 2015, 370, 20140038. [PubMed: 25533095]
38. Schleh C; Rothen-Rutishauser B and Kreyling WG The Influence of Pulmonary Surfactant on Nanoparticulate Drug Delivery Systems. Eur. J. Pharm. Biopharm 2011, 77, 350. [PubMed: 21195761]
39. Yacobi NR; DeMaio L; Xie J; Hamm-Alvarez SF; Borok Z; Kim KJ and Crandall ED Polystyrene Nanoparticle Trafficking across Alveolar Epithelium. Nanomedicine 2008, 4, 139–145. [PubMed: 18375191]
40. Fazlollahi F; Angelow S; Yacobi NR; Marchelletta R; Yu AS; Hamm-Alvarez SF; Borok Z; Kim KJ and Crandall ED Polystyrene Nanoparticle Trafficking across MDCK-II, Nanomedicine 2011, 7, 588–594. [PubMed: 21310266]
41. Lacerda L; Russier J; Pastorin G; Herrero MA; Venturelli E; Dumortier H; Al-Jamal KT; Prato M; Kostarelos K and Bianco A Translocation Mechanisms of Chemically Functionalised Carbon Nanotubes across Plasma Membranes. Biomaterials 2012, 33, 3334–3343. [PubMed: 22289266]
42. Swain RJ; Kemp SJ; Goldstraw P; Tetley TD and Stevens M Assessment of Cell Line Models of Primary Human Cells by Raman Spectral Phenotyping. Biophys. J 2010, 98, 1703. [PubMed: 20409492]
43. Thorley AJ; Grandolfo D; Lim E; Goldstraw P; Young A and Tetley TD Innate Immune Responses to Bacterial Ligands in the Peripheral Human Lung-Role of Alveolar Epithelial TLR Expression and Signaling. PLoS One 2011, 6, e21827. [PubMed: 21789185]
44. Aoyagi T; Terashima O; Nagas Y and Matsui K Preparation of a Polymer Containing Hexadecylpyridinium Bromide Groups and its Utilization as a Transdermal Drug Penetration Enhancer. Polymer 1991, 32, 2106–2111.

45. Coyuco JC; Liu Y; Tan BJ and Chiu GN Functionalized Carbon Nanomaterials: Exploring the Interactions with Caco-2 Cells for Potential Oral Drug Delivery. Int. J. Nanomedicine 2011, 6, 2253–2263. [PubMed: 22125408]

46. Sadekar S and Ghandehari H Transepithelial Transport and Toxicity of PAMAM Dendrimers: Implications for Oral Drug Delivery. Adv. Drug Deliv. Rev 2012, 64, 571–588. [PubMed: 21983078]

47. Shvedova AA; Fabisiak JP; Kisin ER; Murray AR; Roberts JR; Tyurina YY; Antonini JM; Feng WH; Kommineni C; Reynolds J; Barchowsky A; Castranova V and Kagan VE Sequential Exposure to Carbon Nanotubes and Bacteria Enhances Pulmonary Inflammation and Infectivity. Am. J. Respir. Cell Mol. Biol 2008, 38, 579–590. [PubMed: 18096873]

48. Choi HS; Ashitate Y; Lee JH; Kim SH; Matsui A; Insin N; Bawendi MG; Semmler-Behnke M; Frangioni JV and Tsuda A Rapid Translocation of Nanoparticles from the Lung Airspaces to the Body. Nat. Biotechnol 2010, 28, 1300–1303. [PubMed: 21057497]

49. Oberdorster G; Sharp Z; Atudorei V; Elder A; Gelein R; Kreyling W and Cox C Translocation of Inhaled Ultrafine Particles to the Brain. Inhal. Toxicol 2004, 16, 437–445 (2004). [PubMed: 15204759]

50. Smith BW and Luzzi DE Electron Irradiation Effects in Single Wall Carbon Nanotube. J. Appl. Phy 2001, 90, 3509–3515 (2001).

51. Miragoli M; Novak P; Ruenraroengsak P; Shevchuk AI; Korchev YE; Lab MJ; Tetley TD and Gorelik J Functional Interaction between Charged Nanoparticles and Cardiac Tissue: a New Paradigm for Cardiac Arrhythmia? Nanomedicine (Lond) 2013, 8, 725–737. [PubMed: 23140503]

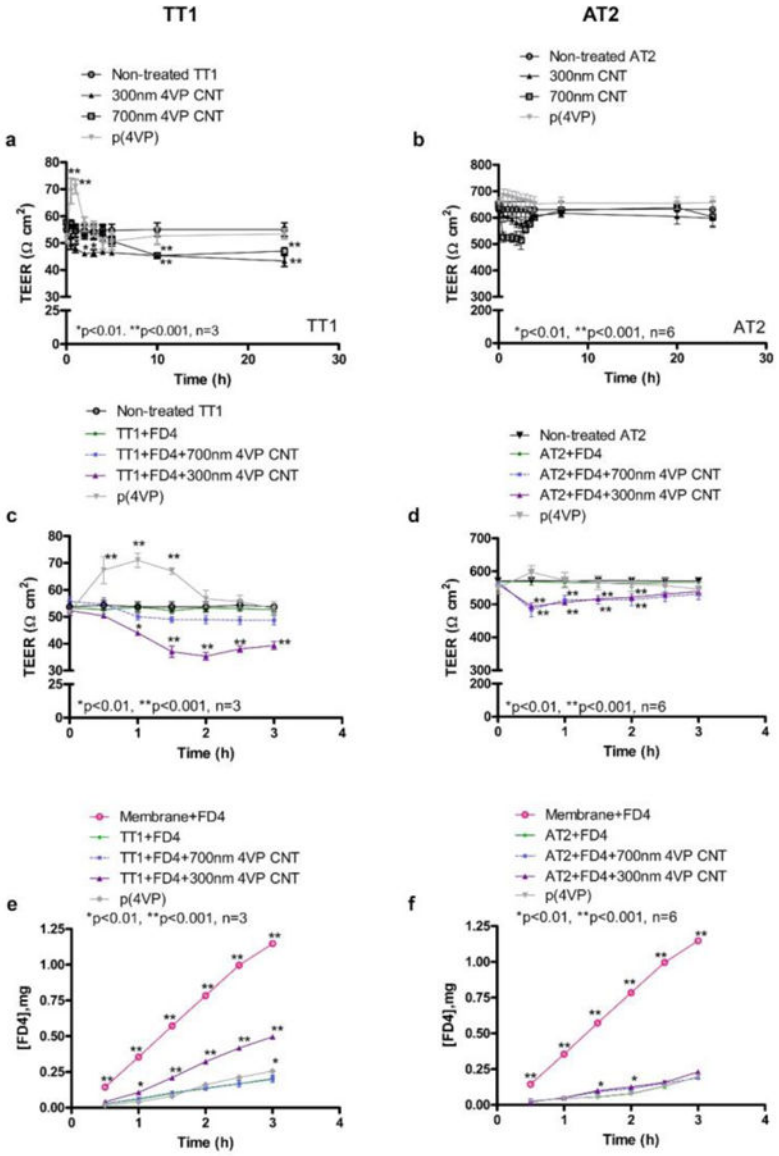

Figure 1.

Effects of p(4VP)-MWCNTs on TEER and dextran transport. The 300 and 700nm p(4VP)-MWCNTs caused a reduction of TEER in a time dependent manner in TT1 (a) and AT2 (b) cells, there was no reduction in TEER in the cells exposed to p(4VP). The TEER promptly decreased during the first 2h of exposure (TT1: a, c; AT2: b, d). (a) The TEER reduction in TT1 cells exposed to 300 and 700nm p(4VP)-MWCNTs did not return to the original values following 24h exposure (*p<0.01,**p<0.001, n=3). (b) In AT2 cells the 300nm p(4VP)-MWCNTs caused TEER reduction at t=0.5–2h and the TEER returned toward the original values after 7h exposure. (c-d) The 300nm p(4VP)-MWCNTs caused significantly higher reduction (*p<0.01, **p<0.001, n=3(TT1), 6(AT2)) in TEER than the 700nm p(4VP)-MWCNTs in both cell types, indicating an effect of the length. (e-f) The 300nm p(4VP)-MWCNTs caused a significant increase (*p<0.01, **p<0.001, n=3(TT1)) in apical-basal

dextran transport in TT1 cells (e), whereas a significant difference in dextran transport was only observed at t=1.5 and 2h in AT2 cells exposed to 300nm p(4VP)-MWCNTs (f).

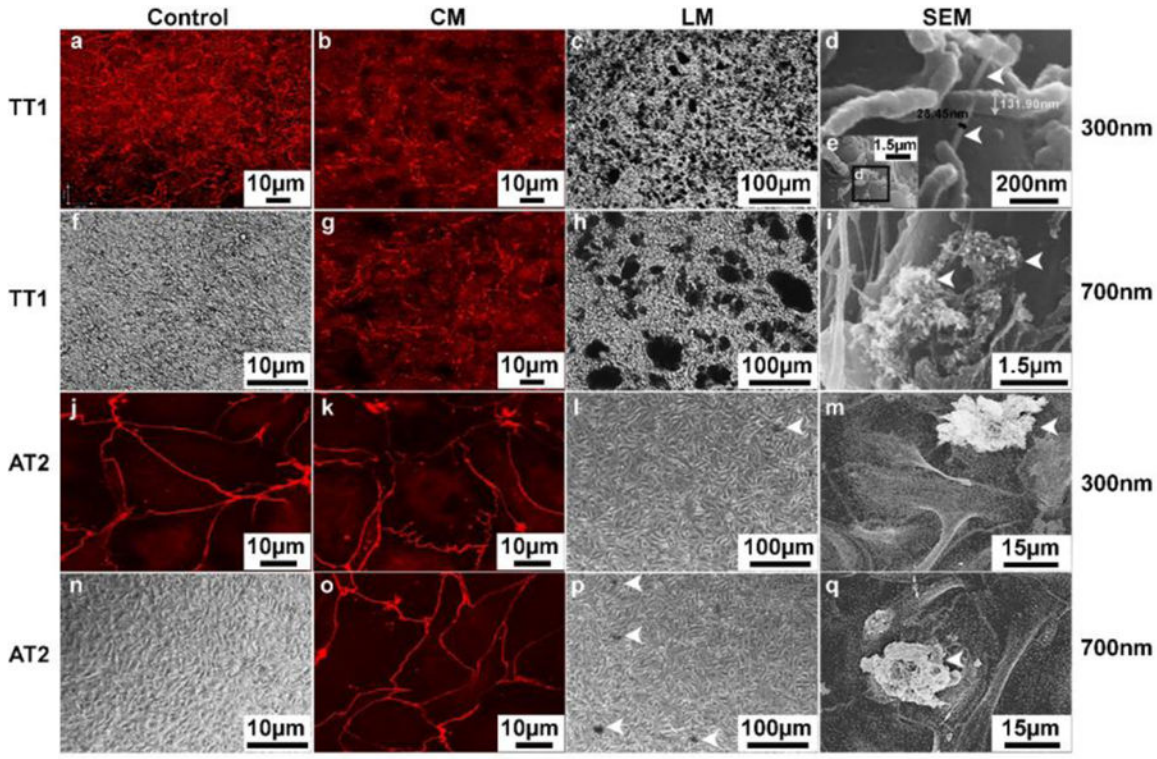

Figure 2.

Interaction between the p(4VP)-MWCNTs and TT1 and AT2 cell monolayers. TT1 and AT2 monolayers visualised using CM (Panels b, g, k, o), LM (Panels c, h, l, p) and SEM (Panels d, e, i, m, q) following 24h p(4VP)-MWCNT exposure (n=3). (a, f, j, n) CM of non-treated control TT1 and AT2 stained with ZO-1 for the tight junctions are shown in a and j (red stain); LM of the non-treated control TT1 and AT2 are shown in panels f and n, respectively. (b, g) A reduction in the intensity of the ZO-1 tight junction proteins was observed with the TT1 cells after 300 (b) and 700nm (g) p(4VP)-MWCNT exposure. (c) LM showed aggregated 300nm p(4VP)-MWCNTs (numerous black patches) adhered to the plasma membrane of TT1 cells; (d-e) SEM identified the individualised 300nm p(4VP)-MWCNTs inserted into plasma membrane (arrows in (d)); (e) low magnification image of d. (h) LM following exposure of TT1 to 700nm p(4VP)-MWCNT exposure showed larger aggregates of 700nm p(4VP)-MWCNTs (large black patches in (h)) than were observed with 300nm p(4VP)-MWCNTs, which were associated with the membrane. (i) SEM image of 700nm p(4VP)-MWCNT aggregates were observed on the plasma membrane of TT1 cells. (k, o) The p(4VP)-MWCNT (300nm (k) and 700nm (o)) caused no change in intensity and tight junction morphology of AT2 cells. (l, p) There were far fewer and smaller aggregates of 300nm (l) and 700nm (p) p(4VP)-MWCNT (arrows indicate the black patches in (l) and (p)). (m, q) SEM of AT2 cell exposed with 300nm (m) and 700nm (q) p(4VP)-MWCNT indicated that the few aggregates that were detected and the aggregates were associated with the plasma membrane of the AT2 cells.

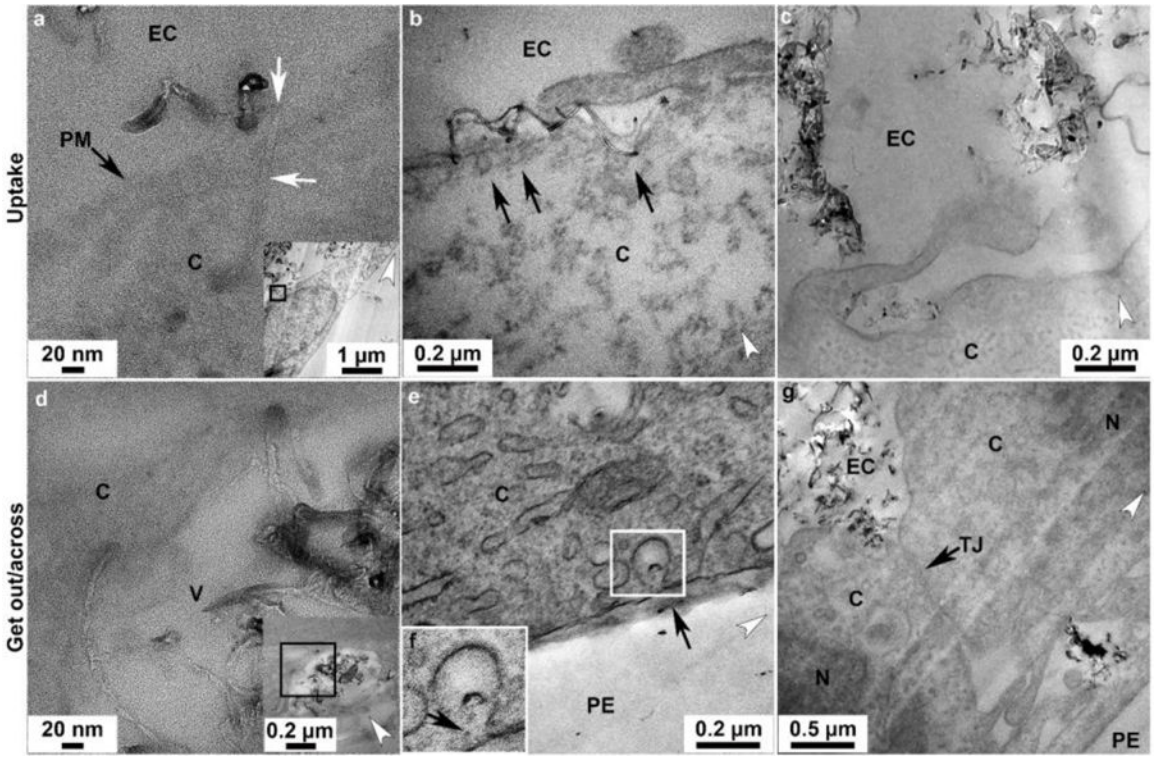

Figure 3.

Transport pathways of p(4VP)-MWCNTs across TT1 monolayers. Similar trends of the uptake and transport were observed with TT1 cells exposed to 300 and 700nm p(4VP)-MWCNTs (see also in Figure 4). For the uptake: (a) HR-TEM image of a 700nm p(4VP)-MWCNTs (white arrows) inserted into the plasma membrane, PM (black arrow); panel a is taken from the boxed region in the inset panel showing the low magnification image of a. (b) Small aggregates of p(4VP)-MWCNTs activated the endocytic cups (arrows in b) prior to uptake by endocytosis. (c) Large aggregated 300nm p(4VP)-MWCNTs were taken up *via* macropinocytosis. (d) TEM imaging showed that 700nm p(4VP)-MWCNTs penetrated through a vesicle membrane (the insert figure shows the low magnification image of d). (e), Individual 300nm p(4VP)-MWCNTs were possibly released out from the vesicle *via* exocytosis at cell basal side (arrows in f). (f) The high magnification of the square in e. (g) The 700nm p(4VP)-MWCNTs were observed above and below the cell tight junction (TJ; arrow in h). EC, N, V, C, TJ and PE denote extracellular region, cell nucleus, vesicle, cytosol, tight junction and polyester membrane support, respectively. The white arrow heads indicate the knife marks and show the cutting direction.

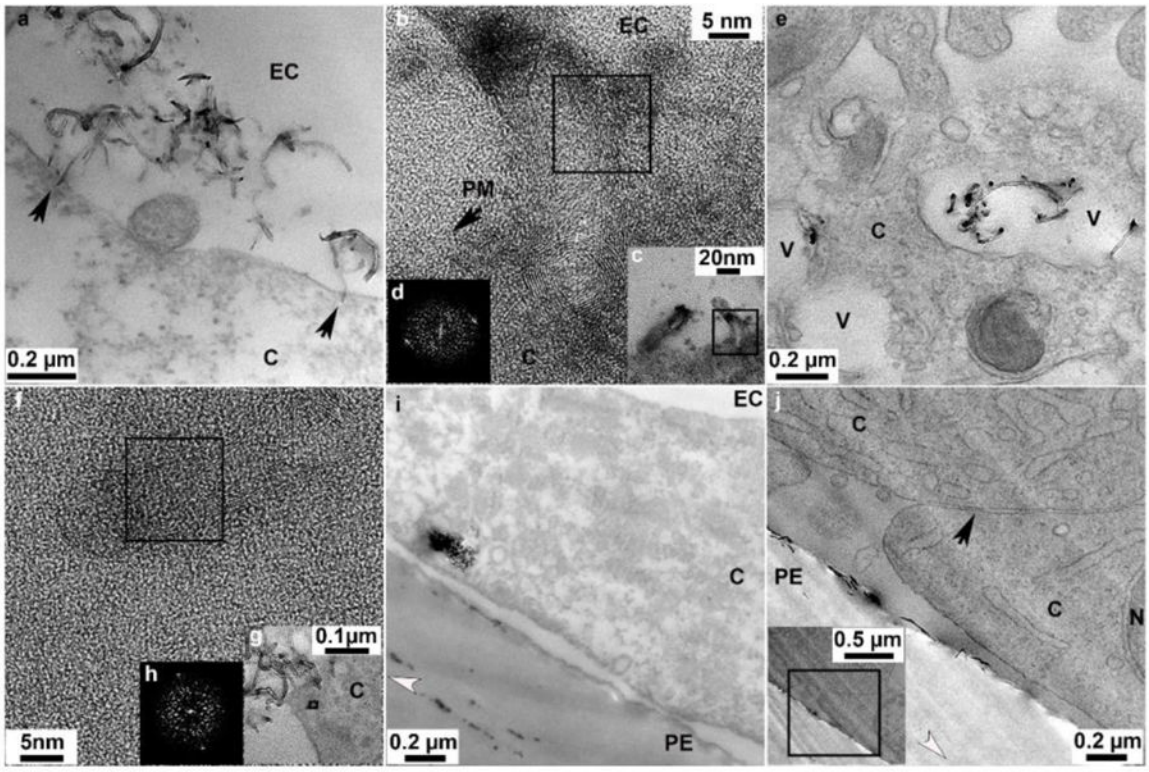

Figure 4.

Uptake and cellular distribution of p(4VP)-MWCNTs within TT1 cells. (a) 700nm p(4VP)-MWCNTs aligned at 90° toward the plasma membrane (arrows) and inserted into the plasma membrane. (b) An HR-TEM image shows 300nm 4VP-MWNCTs penetrated the plasma membrane (PM). (c) Low magnification image of panel b. (d) Fast fourier transform (FFT) of the boxed region on panel b shows crystalline p(4VP)-MWCNT. (e) Individual and aggregated 300nm p(4VP)-MWCNTs inside vesicles within the cell. (f) HR-TEM image of an individual 300nm p(4VP)-MWCNTs within the cell cytoplasm; (g) Low magnification image of panel f. (h) FFT of the boxed region, (h) in panel f shows crystalline p(4VP)-MWCNTs within the cell. (i) Aggregates of 300 nm p(4VP)-MWCNTs at the basal side of the TT1 cell monolayer. (j) 300nm p(4VP)-MWCNTs at cell basal side beyond the cellular tight junction; the insert is the low magnification image of panel j. The black arrow in panel j indicates a tight junction. EC, N, V, C and PE denote extracellular region, cell nucleus, vesicles, cytosol and polyester membrane support, respectively. The white arrow heads indicate knife marks and show the cutting direction.

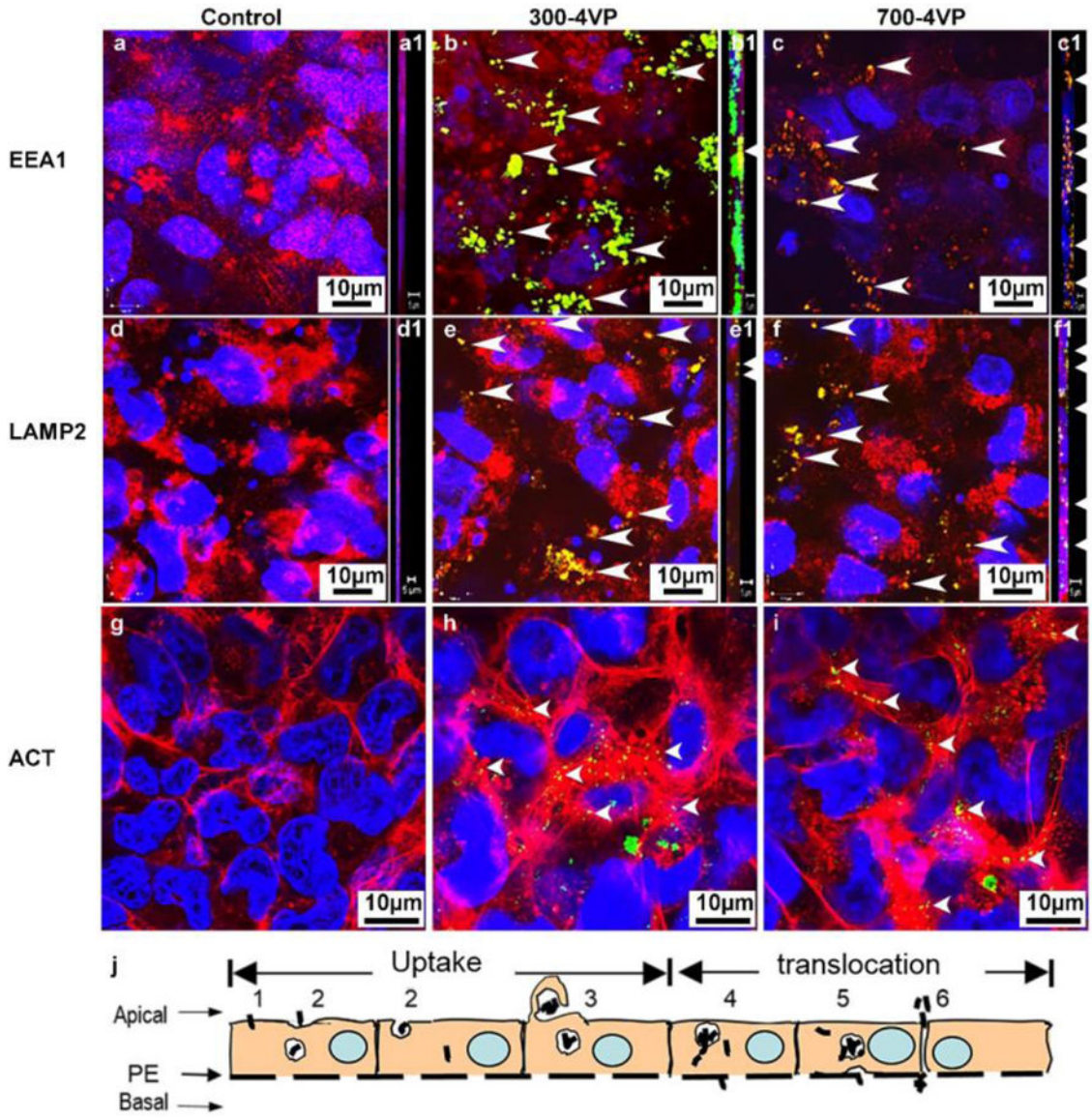

Figure 5.

Uptake mechanisms and cellular distribution of p(4VP)-MWCNTs in TT1 cells. Similar patterns were observed (n=3) with 300 and 700nm p(4VP)-MWCNTS (green). (a-c) Both lengths of p(4VP)-MWCNTs were taken up *via* endocytosis (EEA1 shown in red in a-c) and were observed within endosomes (EEA1 shown in red in a-a1=control, arrow head co-localisation of EEA1 and MWCNTs as yellow areas in b-b1 and c-c1). (d-f) p(4VP)-MWCNTs were also observed within lysosomal compartments of TT1 cells (LAMP2 show in red in d-d1=control, arrow heads indicate co-localisation of lysosomes and MWCNTs as yellow areas in e-e1 and f-f1).The orthoslice images throughout the whole yz-stack images also show the MWCNT co-localisation with EEA1 (yellow in SV6) and LAMP2 (yellow in SV7). (g-i) Non-selective binding (arrows) was observed between actin (red) and 300 and 700nm p(4VP)-MWCNTs (g=control, arrows in panels h-i). (j) Diagram outlining possible transport pathways by which p(4VP)-MWCNTs could enter and cross TT1 cell monolayer:

j1=direct penetration, j2= endocytosis, j3=macropinocytosis, j4= lysosomal penetration and passive diffusion, j5= exocytosis, and j6= paracellular transport, respectively.

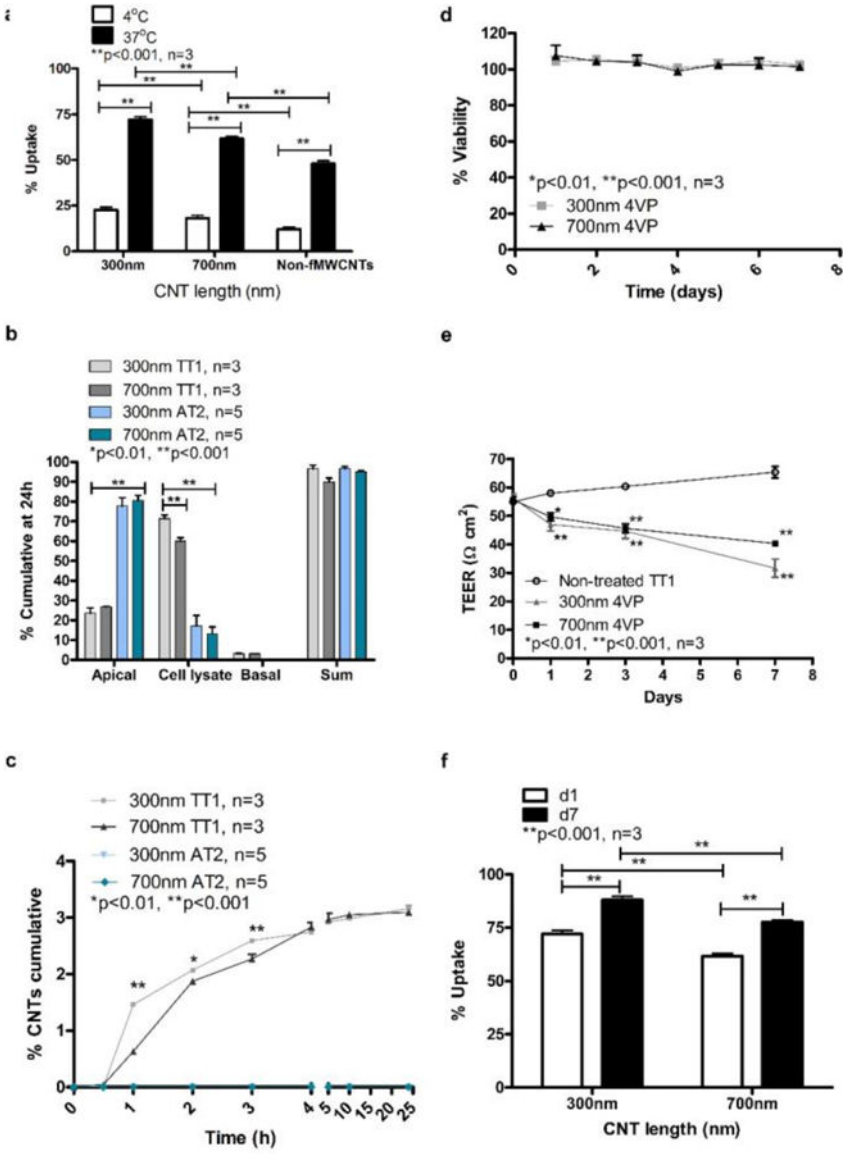

Figure 6.

Translocation of p(4VP)-MWCNTs across alveolar epithelial cell monolayers depends on temperature, cell type and exposure time. (a) Uptake of non-fMWCNTs and p(4VP)-MWCNTs (300nm and 700nm long) by TT1 cells observed at 4 and 37°C. A significant decrease (**p<0.001, n=3 experiments with 300 total observed cells) in percentage of cell uptake of 300 and 700nm p(4VP)-MWCNTs was observed at 4°C. (b) Both the 300 and 700nm p(4VP)-MWCNTs were detected in the basal chambers of the TT1 cell models after 24h exposure. The p(4VP)-MWCNTs did not cross AT2 monolayer (panel b and c; n= 5 subject samples). (c) The rate of p(4VP)-MWCNT transport was plotted against time; there was no translocation across AT2 cells (n=5subject samples). Translocation across TT1 cells increased significantly over 24 hours for both lengths of MWCNTs (*p<0.01,**p<0.001, n=3 experiments). (d) TT1 cell viability was unaffected by 300 and 700nm p(4VP)-MWCNTs over 7 days treatment. (e) TT1 TEER values decreased significantly

(*p<0.01,**p<0.001, n=3) at days 1, 3 and 7. (f) The percent TT1 cell uptake of applied p(4VP)-MWCNTs depended on the length of the p(4VP)-MWCNTs and exposure time. More uptake was observed with 300nm p(4VP)-MWCNTs (d;**p<0.001, n=3 experiments), and cell uptake increased as a function of time in TT1 cells.

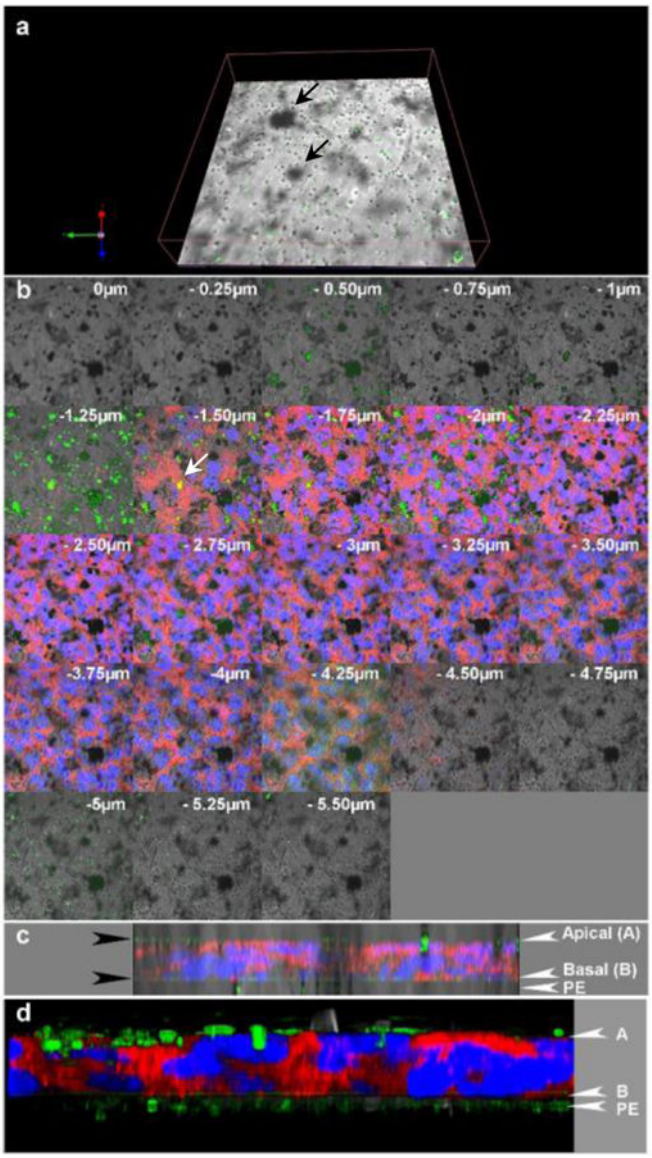

Figure 7.

Distribution of 300nm long p(4VP)-MWCNTs across a TT1 cell monolayer at 24h following apical application. (a) Confocal image showing the p(4VP)-MWCNTs (green) at the basal side of the cell, within the supporting polyester membrane (PE), many located at membrane pores (section −4.75 to −5μm in panel b). The 4VP-MWNTs are green in the reflecting channel and they can be seen as black patches in the transmission channel. (b) Translocation of p(4VP)-MWCNTs across the TT1-monolayer (blue=nuclei and red=plasma membrane); the stack was 0.25 μm thick and the value on each image indicates focal height of the image along the z-axis. Aggregated p(4VP)-MWCNTs (green and black patches in b) were observed within the TT1-monolayer and some MWCNTs co-localised with the cell cytoplasm (yellow in panel b at z= −1.5 and −1.75). (c-d) 3D images of stack images from 4 channels: green, red, blue with (c) /without transmission channel (d) were combined and illustrated in yz-plane. The green layer on the top and at the basal side of cell monolayer

(black arrows in c) indicate the aggregated p(4VP)-MWCNTs adhered on the apical side of the cell and the p(4VP)-MWCNTs crossed the monolayer which were trapped by the supporting transwell membrane (PE), respectively.

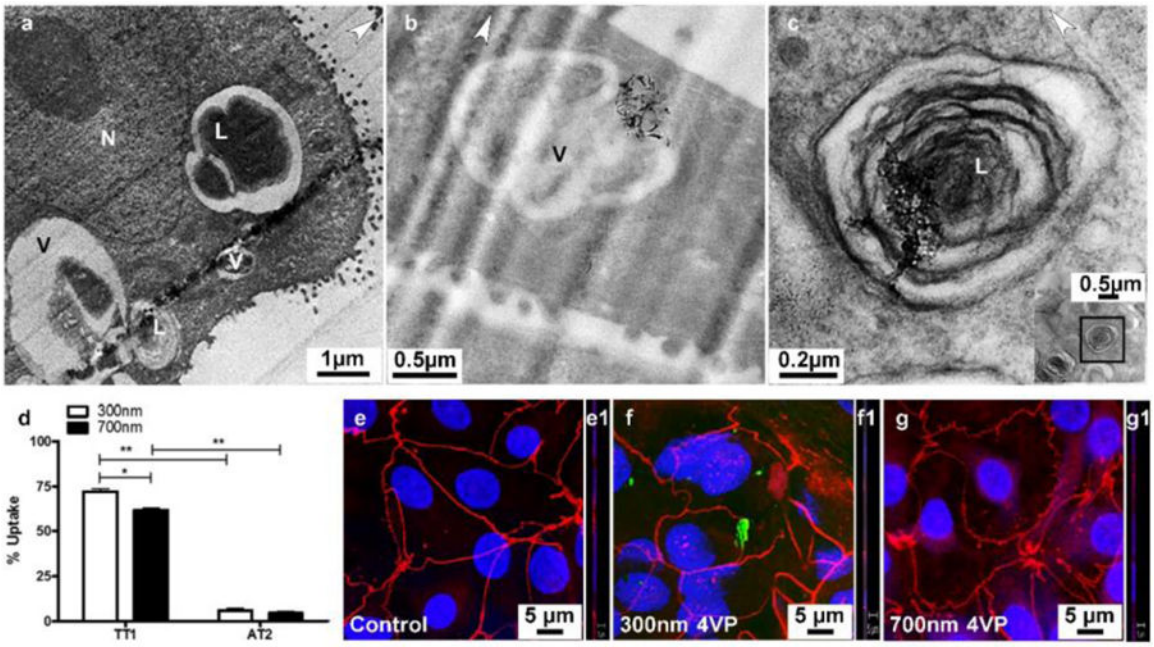

Figure 8.

Uptake of p(4VP)-MWCNTs by AT2 cells. (a) AT2 cells are secretory cells and their unique lamellar bodies (L), were observed in TEM images. (b) The p(4VP)-MWCNTs were rarely observed within AT2 cells, but they were mostly found as agglomerates/aggregates possibly taken up *via* endocytosis by AT2 cells (SV9–10). (c) During recycling of surfactant, some aggregated p(4VP)-MWCNTs were also observed in lamellar bodies; the insert is low magnification of panel c showing cell cytoplasm of AT2 cell. The white arrow heads indicate the knife marks in the section and show the cutting direction. L, N and V are a lamellar body, cell nucleus and vesicle. (d) In comparison to TT1 cells, uptake of p(4VP)-MWCNT by AT2 cells was found to be much lower following 24h exposure. The percentage uptake of p(4VP)-MWCNTs (300 and 700nm) in AT2 cells was 4–8% (panel d), whereas, uptake of 300 and 700nm p(4VP)-MWCNTs in TT1 cells was 72 and 62%, respectively (*$p<0.01$,*$p<0.001$, n=300 total cells surveyed). (e-g) Both 300 (f) and 700nm (g) p(4VP)-MWCNTs caused no changes to structural continuity of the tight junctions (OZ-1 in red) in AT2 cells.